Chapter 11
NOMA in Vehicular Communications

Yingyang Chen, Li Wang, Yutong Ai, Bingli Jiao and Lajos Hanzo

11.1 Background and Motivation

With the rapid development of intelligent transportation systems (ITS), the broad objective of vehicular communications is to improve the travel experience of users. To support a variety ITS applications, the integrated vehicular networking concept termed as 'vehicle-to-everything' (V2X) has been proposed. To elaborate a little further, this includes four main types of communications, namely vehicle-to-vehicle (V2V), vehicle-to-pedestrian (V2P), vehicle-to-infrastructure (V2I), and vehicle-to-network (V2N) scenarios, where the ultimate objective is that of offering improved road safety, traffic efficiency, and infotainment services [1].

The IEEE 802.11p standard was conceived in support of wireless access for vehicular environments (WAVE), specifically dedicated to vehicular safety applications and to the provision of data rates ranging from 6 to 27 Mbps for short-transmission distances [2]. However, 802.11p fails to support flexible scalability and to provide quality of service (QoS) guarantees. Furthermore, it has a potentially unbounded delay. These characteristics of the IEEE 802.11p standard prevent its employment in demanding V2X services requiring low latency and high reliability [3, 4]. Moreover,

Y. Chen · B. Jiao
School of Electronics Engineering and Computer Science, Peking University,
Beijing 100871, China
e-mail: chenyingyang@pku.edu.cn

B. Jiao
e-mail: jiaobl@pku.edu.cn

L. Wang (✉) · Y. Ai
School of Electronic Engineering, Beijing University of Posts and Telecommunications,
Beijing 100876, China
e-mail: liwang@bupt.edu.cn

Y. Ai
e-mail: ytailiwang@bupt.edu.cn

L. Hanzo
School of Electronics and Computer Science, University of Southampton,
Southampton SO17 1BJ, U.K.
e-mail: lh@ecs.soton.ac.uk

M. Vaezi et al. (eds.), *Multiple Access Techniques for 5G Wireless Networks and Beyond*, https://doi.org/10.1007/978-3-319-92090-0_11

due to the asynchronous nature of the IEEE 802.11p transmission, its performance is inevitably degraded by the packet collisions imposed by the hidden node problem encountered in carrier sense multiple access with collision avoidance (CSMA/CA) solutions. Finally, the current status of IEEE 802.11p does not support an evolutionary path for improving its reliability, robustness, and coverage [5].

As an alternative to the IEEE 802.11p-based vehicular ad hoc network (VANET) concept, the long-term evolution (LTE)-based V2X solution has been actively developed by the 3rd Generation Partnership Project (3GPP), and it was redefined as LTE V2X within the 3GPP standardization framework so as to provide a beneficial solution for V2X communications [6]. As a benefit of the global deployment and commercialization of LTE systems, LTE V2X serves as an integrated solution for vehicular communications. To be more specific, given an LTE network, both V2I and V2N services can be supported at a high data rate, whilst maintaining an excellent QoS with the aid of the so-called eNodeBs. Meanwhile, LTE can be extended to support V2V and V2P services by invoking direct device-to-device (D2D) communications for satisfying the QoS requirements even in the case of high vehicular densities [7]. Finally, in contrast to 802.11p, the hidden node problem can be avoided in LTE V2X scenario due to its synchronous nature, whilst both the reliability and latency can also be improved.

The rest of this section is organized as follows. First, we provide an overview of existing LTE-based V2X systems. Then, we describe the applicability of a range of popular transmission techniques to vehicular communications. A non-orthogonal multiple access (NOMA) and spatial modulation (SM)-based transmission scheme are proposed for supporting the high data rate and high-reliability demands of V2X systems. Finally, we detail the outline of this chapter.

11.1.1 Overview of LTE-Based V2X

11.1.1.1 Typical V2X Services

The operational LTE system is already capable of supporting ITS applications. The V2X services can be broadly classified into three typical types, namely *road safety*, *traffic efficiency*, and *infotainment* enhancement applications [1, 8]. *Road safety* enhancements aim for reducing the risk of accidents and hence have to satisfy stringent reliability and latency specifications. Basically, the road safety services are short messages and periodically broadcast from each vehicle to its neighbours within a particular geographic region.

As the second category of vehicular applications, *traffic efficiency* enhancements aim for optimizing the platooning of vehicles by reducing traffic congestion. The vehicles are required to collect sensed data and send them to the remote management servers for route planning. Although the reliability and delay requirements related to traffic efficiency enhancements are less strict than those of the safety enhance-

ments, it is still necessary to keep the packet loss and latency low in high-velocity environments.

In contrast to the previous two categories, *infotainment* services include a range of traditional and emerging Internet applications, such as popular content download and dissemination, social networking, and Web browsing, with the goal of providing an improved driving experience.

11.1.1.2 LTE-Based V2X Communication Modes

To support key applications in vehicular communications, the LTE system offers a pair of communication modes.

LTE D2D for V2V/V2P: Although the original system does not support V2V/V2P communications natively, LTE has been extended to support V2V/V2P direct communications based on a device-to-device (D2D) sidelink design through the so-called PC5 interface [7]. The LTE D2D mode allows the terminals in close proximity of each other to communicate directly without involving the base stations. As a benefit, the end-to-end latency can be reduced for satisfying the associated QoS requirements. At the time of writing, the LTE D2D mechanism is considered as the baseline for PC5-based V2V/V2P communications [9]. However, in high user density scenarios, the attributes of V2X services are different from those of the legacy LTE D2D communications, since V2X services are periodic or event-triggered. Hence, efficient resource allocation has to be conceived for dense, high-mobility scenarios.

Cellular LTE for V2I/V2N: Cellular LTE refers to the common communication mode between vehicles and infrastructure/network units. Specifically, there are two main cellular LTE mechanisms, namely *unicast* and *multicast*. In the case of *unicast*, the vehicles are addressed individually. By contrast, in the *multicast* case, all vehicles in the relevant area are collectively addressed. LTE supports high-quality multicast and transmissions through the evolved multimedia broadcast multicast service (eMBMS) capabilities in the radio access network [10]. Compared to unicast services, multicast offers the capability of geocasting the data to a set of users more resource efficiently, although at the cost of longer delays due to the cumbersome eMBMS session set-up, especially in the face of a heavy traffic load.

11.1.1.3 LTE-Challenges in Vehicular Scenarios

The LTE system is capable of providing a round-trip delay below 10 ms and a radio access latency of less than 100 ms. It is based on orthogonal frequency-division multiple access (OFDMA) in the downlink and single-carrier frequency-division multiple access (SC-FDMA) in the uplink. It exhibits flexible resource allocation and scheduling. The LTE system also relies on multiple-input multiple-output (MIMO) techniques for improving the diversity and/or multiplexing gain of the previous generations, making LTE attractive in dynamic vehicular wireless propagation environments.

However, the ever-growing demands for vehicular communications increase the tele-traffic congestion. Hence, it is desirable to achieve a **high bandwidth efficiency, massive connectivity, high reliability, and low latency** in V2X communications. One of the limitations of the LTE systems arises from the fact that LTE was designed for supporting the user terminals sharing the wireless resources using orthogonal multiple access (OMA), which can be potentially improved by NOMA schemes in V2X communications.

In order to support advanced V2X services, given their stringent reliability and latency requirements, multiple-input multiple-output (MIMO) techniques may be invoked. Traditionally, MIMO schemes have been designed either for enhancing the diversity gain by combating the channel fading (e.g. Alamouti code), or for spatial multiplexing (e.g. Vertical Bell Laboratories Layered Space-Time, termed VBLAST), albeit they are amalgamated by the multi-functional MIMO concept of [11, 12]. To accommodate the ever-increasing demands of multimedia services and applications, the massive MIMO concept emerged [13, 14]. Theoretically, massive MIMO is able to reap all the benefits of conventional MIMO and offers abundant degrees of freedom (DoFs). By exploiting the knowledge of the channel state information at the transmitter (CSIT), a massive antenna array becomes capable of simultaneously serving a large number of users by sharing its multiplexing gain among them, while providing higher data rates and transmission reliability. Furthermore, in contrast to shirt-pocket-sized handsets, the employment of large-scale MIMO schemes becomes realistic in V2X scenarios, since multiple antennas can be realistically accommodated [15, 16].

However, massive MIMOs suffer from various problems, including the inter-antenna interference (IAI) and the high complexity of the receivers. It would be a particularly costly process to acquire CSIT in frequency-division duplexing (FDD) systems. Moreover, the hardware cost (e.g. a dedicated radio frequency (RF) chain associated with each antenna) becomes excessive for large antenna arrays. In vehicular wireless communications, the gravest challenge is the hostile high-Doppler propagation imposed. For example, the dominant Doppler effect aggravates the inter-subcarrier interference of orthogonal frequency-division multiplexing (OFDM), and the strong line of sight (LoS) component of V2V channels would aggravate the spatial correlation between antennas. Therefore, the direct applications of massive MIMO in vehicular transmissions are deemed to be problematic, and another version of massive antenna technology is required to be fit for LTE V2X communications.

11.1.2 The Applicability of NOMA to V2X Communications

To mitigate the probability of access collision in V2X environments, a range of novel multiple access techniques has been proposed, such as sparse code multiple access (SCMA), pattern division multiple access (PDMA), and non-orthogonal multiple access (NOMA) to support higher bandwidth efficiency and massive connectivity [17, 18]. Among these techniques, NOMA exhibits an appealing low receiver complexity,

high bandwidth efficiency, and massive connectivity by allowing multiple users to share the same channel resource via power domain multiplexing. Thus, NOMA is considered to be a promising candidate for future wireless access [19]. To mitigate the multiple access interference (MAI), multi-user detection (MUD) techniques such as successive interference cancellation (SIC) [20] can be applied to the end-user receivers for detecting the desired signals. Through power domain multiplexing at the transmitter and SIC at the receivers, NOMA becomes capable of fully exploiting its capacity region hence outperforming the OMA schemes [21].

The specific design aspects of NOMA schemes in cellular environments have been discussed in [22–24]. Explicitly, in [22], the concept of basic NOMA with SIC was introduced and its performance was compared to that of the traditional orthogonal frequency-division multiple access (OFDMA) scheme through a system-level evaluation. A beneficial power allocation scheme was designed in [23] for striking compelling tradeoffs between the user fairness and system throughput. Lv et al. [24] studied a new cooperative NOMA transmission scheme and derived the outage probability associated with fixed power allocation.

In vehicular environments, NOMA provides a new dimension for V2X services to alleviate the access collisions, thereby improving the bandwidth efficiency as well as supporting massive connectivity. The authors of [25] proposed an contention-based uplink NOMA solution in order to reduce the control signalling overhead. In [26], the NOMA concept was exploited to enhance the transmission of safety information, which required low latency and high reliability within a dense vehicular communication network. The authors of [27] invoked the NOMA principle for boosting the bandwidth efficiency of the infotainment applications in V2X services. In conclusion, NOMA is eminently applicable for supporting V2X services with enhanced bandwidth efficiency and QoS support.

11.1.3 The Applicability of SM to V2X Communications

In recent years, spatial modulation (SM) [28] has grown in popularity, because in contrast to the traditional MIMO configurations, it only activates a single transmit antenna (Tx) at every transmission instance. Hence, it only requires a single-RF chain. As a benefit, the inter-antenna interference (IAI) can be completely eliminated. Thus, a reduced implementational cost and complexity are achieved [29, 30].

The basic idea of SM was initially derived from Chau and Yu's work dating back to 2001 [31], where the receiver decodes the signals transmitted from different antennas. Then, a compelling SM-MIMO solution was proposed by Mesleh et al. in [32]. Since then, SM has been extensively studied in the scenario of point-to-point communications. In [28], the authors studied the channel capacity of the SM system under the parlance of information-guided channel hopping (IGCH). It was shown that IGCH provides better spectral efficiency than orthogonal space-time block coding (OSTBC). In [33], the SM concept was studied by using a low-complexity two-stage demodulator, and the potential advantages of SM-MIMO compared to the exist-

ing spatial-multiplexing and Alamouti schemes were shown. In [34], Jeganathan et al. developed the maximum likelihood (ML)-optimum demodulator for SM-MIMO and a range of performance improvements was shown compared to the suboptimal demodulator introduced in [33].

The SM philosophy is that not only the classic quadrature amplitude modulation (QAM) symbols but also the index of the active Tx (spatial constellation) convey information for the sake of achieving bandwidth efficiency enhancements without sacrificing the advantages of a single-RF stage. Consequently, SM was proposed to be combined with massive MIMOs, yielding the novel concept of massive SM-MIMO, where each UE still has one RF chain combined with a massive Tx configuration [35, 36, 38]. Due to the single-RF structure of SM, both the cost and the design complexity of each user terminal remain similar to those of SM-MIMOs, while the data rates can be boosted by conveying more information bits via employing a large Tx array. More specifically, a large-scale multi-user SM-MIMO system was proposed in [35] along with multi-user detection (MUD) schemes. In [36], Wang et al. proposed an uplink transceiver scheme for massive SM-MIMO within frequency-selective fading environments. The authors of [37] investigated the achievable uplink spectral efficiency in a multi-cell massive SM-MIMO scenario, and [38] further investigated the optimal number of Txs at the user equipment.

Indeed, a recent survey of SM can be found in [39]. In [40–43], SM and its extensions were considered in vehicular environments. A differential SM scheme was proposed for vehicle communications in [40], exhibiting robustness against time-selective fading and Doppler effects. Fu et al. [41] studied the bit error rate (BER) performance of SM under a three-dimensional V2V channel model. Peppas et al. [42] applied space shift keying (SSK) in inter-vehicular communications and derived a closed-form expression for the pairwise error probability. In [43], the performance of massive SM-MIMO over a spatio-temporally correlated Rician channel was analysed under a high-speed railway scenario. Moreover, Cui and Fang have demonstrated that by activating a single Tx, SM is capable of alleviating the channel correlation. In conclusion, SM has become increasingly appealing for V2V systems.

11.1.4 NOMA-SM Tailored for Vehicular Communications

Let us continue by conceiving a novel transmission scheme, termed NOMA-SM, by intrinsically amalgamating NOMA and SM in support of vehicular communications [27]. Specifically, in synergy with the inherent requirement of high bandwidth efficiency, NOMA is invoked for non-orthogonally accessing all the resources combined with the single-RF benefits of SM. The bandwidth efficiency of the proposed NOMA-SM scheme is further boosted by a massive Tx configuration.

Against this background, the key points of the proposed scheme are threefold: firstly, the novel NOMA-SM concept is proposed and its link reliability is quantified. Secondly, the capacity of NOMA-SM is derived and verified by Monte Carlo

simulations. Thirdly, a pair of upper bounds on the capacity of NOMA-SM is formulated in closed form and a power allocation optimization is considered.

Explicitly, instead of simply combining a pair of popular techniques, their benefits are intrinsically amalgamated. By investigating the BER performance of NOMA in comparison to different MIMO techniques and the bandwidth efficiency of SM combined with distinct multiple access methods, NOMA and SM are shown to cooperatively improve V2V transmissions.

11.1.5 Outline of the Chapter

The rest of this chapter is organized as follows. In Sect. 11.2, the system model of NOMA-SM is presented, while Sect. 11.3 provides the capacity analysis and mutual information (MI) evaluation of NOMA-SM. Our capacity upper bound derivations and power allocation problem are considered in Sect. 11.4. Simulation results and discussions of the BER performance are provided in Sect. 11.5, together with the numerical capacity analysis and power allocation optimization. In the final section, we offer the main conclusions of this chapter and discuss some open problems as well as a range of promising potential research directions. For convenience, we list the most important notations here.

Notation: Uppercase and lowercase bold-faced letters indicate matrices and vectors, respectively. $(\cdot)^{-1}$, $(\cdot)^{H}$, $\det(\cdot)$, and $[\cdot]_{p,q}$ represent inverse, conjugate-transpose, determinant, and the entry in the pth row and q-column of a matrix, respectively. $\mathbb{E}_X\{\cdot\}$ denotes the expectation on the random variable X. $\mathbf{A} \in \mathbb{C}^{M\times N}$ is a complex-element matrix with dimensions $M \times N$, and $\mathbf{I}_N$ is an $N \times N$ identity matrix. $|\cdot|$ and $(\cdot)^*$ imply the absolute value and the conjugate of a complex scalar, while $\|\cdot\|$ denotes the Euclidean norm of a vector. Finally, $x \sim \mathcal{CN}\left(\mu, \sigma^2\right)$ indicates that the random variable x obeys a complex Gaussian distribution with mean μ and variance σ^2.

11.2 System Model

We consider a generic vehicular communication system, where the vehicle-to-infrastructure (V2I), V2V, and intra-vehicle transmissions are all included. As shown in Fig. 11.1, a base station (BS) is located at the roadside while the vehicles V_1 and V_2 are in motion. There is a mobile user U in V_1 who requests to download a file locally cached at the BS. Vehicle V_2 also requests to download its own intended signal from BS. We assume that V_1 has also acquired the signal of V_2, as a result of the first transmission phase, during which the messages of V_1 and V_2 are transmitted simultaneously from the BS. For example, BS employs a NOMA technique to multiplex signals of V_1 and V_2 in the power domain. By involving the classical SIC, V_1 extracts the signal of V_2 in the spirit of cooperation. Another appropriate interpre-

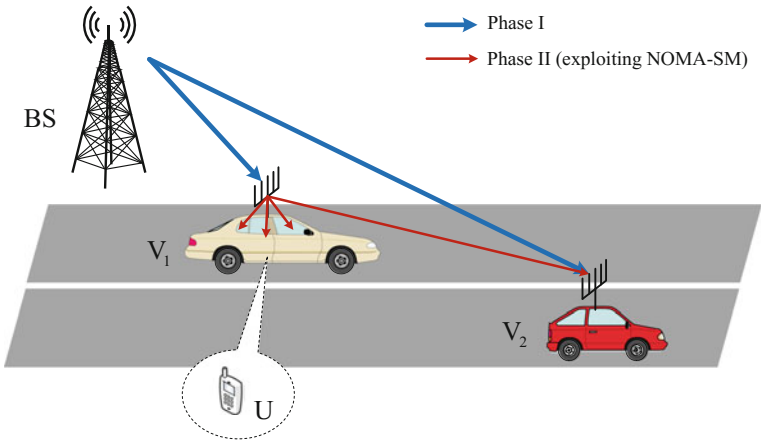

Fig. 11.1 An illustration of the considered vehicular communication system, where NOMA-SM is applied in Phase II

tation is related to the distribution of popular multimedia contents in VANET [44], using peer-to-peer protocols for exchanging popular packets through V2V channels.

Therefore, as shown in Fig. 11.1, cooperative inter-vehicle transmission is constructed during the second phase to enhance the reception reliability. Specifically, V_1 forwards the desired signal to V_2 for cooperatively enhancing the reception at V_2. Furthermore, the second phase scenario can be generalized to various situations. For example, user U can be a roadside unit, aiming for exchanging information with the onboard unit of the vehicle V_1. While U may be a vehicle which is much closer to V_1 than V_2. Similar to the concept in [45], a VANET is formed among these vehicles for exchanging safety information, or for cooperatively distributing popular multimedia contents within a geographical area of interest. In general, our model is valid in a wide range of vehicular scenarios.

In the light of bandwidth scarcity, cognitive radio techniques can be exploited in the second stage to opportunistically exploit the spectrum holes in the licensed spectrum. For example, V_1 may be permitted to share the cellular uplink, for which the data traffic is typically lighter than for the downlink, hence resulting in potential spectrum wastage [46]. Basically, underlay cognitive transmission is feasible without traversing through the primary network. However, the interference imposed by V_1 on the BS in the second stage should be carefully managed, albeit this is beyond the scope of this article. Our main focus is on the second stage of the cooperative transmission in Fig. 11.1, since the performance in the first phase can be analysed similarly. Particularly, the NOMA-SM strategy is employed in the second stage for both V_1–V_2 and V_1–U links.

The schematic diagram of NOMA-SM operated in the second stage is presented in Fig. 11.2, where V_1 assigns distinct transmit power to V_2 and U. The user access is based on NOMA, combined with SM. Although there is the literature proposing

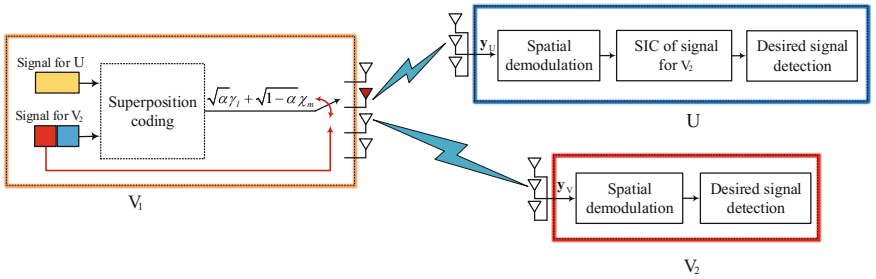

Fig. 11.2 The schematic diagram of the proposed NOMA-SM strategy

multi-user SM schemes [47, 48], we use a classical SM designed for point-to-point transmission [28, 49] in vehicular environments. In what follows, we first elaborate on the principles of the proposed NOMA-SM scheme. Then, our V2V channel model is detailed.

11.2.1 The Principles of NOMA-SM

Let us assume that N_t, N_r, and N_u omnidirectional antennas are employed at V_1, V_2, and U, respectively. As illustrated in Fig. 11.2, the proposed NOMA-SM strategy is applied both for the V_1–V_2 and V_1–U links. At the transmitter V_1, two independent bit streams are prepared for transmission. The bit stream for V_2 is partitioned into two parts: the first $\log_2(N_t)$ bits are used for Tx activation, activating a specific Tx index n_t ($n_t \in \{1, \ldots, N_t\}$). The other $\log_2(M)$ bits destined for V_2 are combined with $\log_2(L)$ bits for U, employing superposition coding.

Subsequently, the modulated symbol $\sqrt{\alpha}\gamma_l + \sqrt{1-\alpha}\chi_m$ is radiated from the activated Tx n_t, where γ_l and χ_m are intended for the in-car user U of V_1 and for V_2, respectively, satisfying $\mathbb{E}\{|\gamma_l|^2\} = \mathbb{E}\{|\chi_m|^2\} = E_s$, where E_s is the average energy per transmission at V_1, while α is the power allocation factor. According to the NOMA principle [23], the transmit power of the distant user in Fig. 11.2 must be higher than that of the close-by user, that is $(1-\alpha)E_s > \alpha E_s$. With this, $0 < \alpha < \frac{1}{2}$ should be guaranteed since the in-car user has a good channel. As a result, a block of $\log_2(N_t M L)$ bits unambiguously identifies the active Tx n_t and the superimposed complex symbol $\sqrt{\alpha}\gamma_l + \sqrt{1-\alpha}\chi_m$ transmitted from it. Hence, a NOMA-SM super symbol can be expressed as

$$\mathbf{x} = \mathbf{e}_{n_t}\left(\sqrt{\alpha}\gamma_l + \sqrt{1-\alpha}\chi_m\right),$$

where $\mathbf{e}_{n_t}$ is the n_tth column of the identity matrix $\mathbf{I}_{N_t}$, indicating that the n_tth Tx of V_1 is activated, while the other $(N_t - 1)$ Txs are deactivated. Furthermore, χ_m is

the mth symbol in the M-ary amplitude-phase modulation (APM) used for V_1–V_2 transmission, while γ_l is the lth symbol in the L-ary APM for V_1–U transmission.

Considering the propagation inside the vehicle V_1, we assume that the in-car user U experiences a frequency-flat Rayleigh channel. For example, the Txs of V_1 are installed on the central column of the vehicular dashboard, while the receive antennas (RAs) of U are placed behind the passenger front seat, without LoS from V_1. In [50], this scenario has been shown to be well suited to characterize diffuse scattering. Thus, we let $\mathbf{G} \in \mathbb{C}^{N_r \times N_t}$ denote the channel matrix between V_1 and U, and assume that all entries of $\mathbf{G}$ are independent identically distributed (i.i.d), obeying the distribution $\mathscr{CN}(0, 1)$. The signal vector received at U and V_2 can be written as

$$\mathbf{y}_{\mathrm{U}} = \mathbf{g}_{n_t}\left(\sqrt{\alpha}\gamma_l + \sqrt{1-\alpha}\chi_m\right) + \mathbf{w}_{\mathrm{U}}, \tag{11.1}$$

$$\mathbf{y}_{\mathrm{V}} = \sqrt{p_0}\mathbf{h}_{n_t}\left(\sqrt{\alpha}\gamma_l + \sqrt{1-\alpha}\chi_m\right) + \mathbf{w}_{\mathrm{V}}, \tag{11.2}$$

respectively, where p_0 represents the average power drop between V_1 and V_2 due to the large-scale fading. Furthermore, $\mathbf{g}_{n_t} \in \mathbb{C}^{N_u \times 1}$ is the n_tth column of $\mathbf{G}$, representing the channel vector between U and the n_tth Tx of V_1, while $\mathbf{h}_{n_t} \in \mathbb{C}^{N_r \times 1}$ is the n_tth column of the V2V channel matrix $\mathbf{H} \in \mathbb{C}^{N_r \times N_t}$, indicating the complex fading envelope between V_2 and the n_tth Tx of V_1. Finally, $\mathbf{w}_{(\cdot)}$ denotes a complex additive white Gaussian noise (AWGN) vector with a power spectrum density of σ_0^2 per entry. For the inter-vehicle channel, the path loss is considerable in (11.2), while it is neglected between the in-car user and the antenna array of V_1.

In our system, the transmitter and both receivers are assumed to have perfect synchronization in both time and frequency. Full channel state information is assumed to be available at receivers (i.e. CSIR). In principle, both V_2 and U first have to detect the signal destined for V_2, i.e. the activated Tx index $\hat{n}_t$ and the APM symbol $\chi_{\hat{m}}$ at each particular time instant. The corresponding optimum maximum likelihood (ML) detector is invoked at U and V_2 according to

$$\left(\hat{n}_t, \chi_{\hat{m}}\right) = \arg\min_{n_t, m} \left\| \mathbf{y}_U - \sqrt{1-\alpha}\mathbf{g}_{n_t}\chi_m \right\|^2, \tag{11.3}$$

$$\left(\hat{n}_t, \chi_{\hat{m}}\right) = \arg\min_{n_t, m} \left\| \mathbf{y}_V - \sqrt{p_0\,(1-\alpha)}\mathbf{h}_{n_t}\chi_m \right\|^2. \tag{11.4}$$

After eliminating the interference imposed by $\left(\hat{n}_t, \chi_{\hat{m}}\right)$ on $\mathbf{y}_{\mathrm{U}}$, U becomes capable of performing another ML detection to acquire the desired signal $\gamma_{\hat{l}}$.

11.2.2 V2V Massive MIMO Channel Model

In contrast to the conventional fixed-to-mobile cellular radio systems, in V2V systems, both the transmitter and receiver are in motion and both are equipped with low-elevation antennas, which will result in quite different propagation conditions. Hence, a non-isotropic scattering V2V stochastic model was proposed in [51] for characterizing a wide variety of V2V scenarios by adjusting relevant model parameters. In [41], a novel three-dimensional V2V geometry-based stochastic channel was proposed for accurately capturing the effect of vehicular traffic density on the channel.

In this article, we consider a spatio-temporally correlated Rician channel model for characterizing our narrowband V2V massive MIMO channel, which has also been exploited in [43] and [52]. We describe the underlying V2V channel as a matrix of complex fading envelopes, i.e. $\mathbf{H} \in \mathbb{C}^{N_t \times N_r}$, which can be expressed as

$$\mathbf{H} = \sqrt{\frac{K}{K+1}}\bar{\mathbf{H}} + \sqrt{\frac{1}{K+1}}\tilde{\mathbf{H}},$$

where K is the Rician factor, while $\bar{\mathbf{H}}$ is the fixed part related to the LoS component. Furthermore, $\tilde{\mathbf{H}}$ represents the variable part, whose entries are correlated complex Gaussian variables. Given $\left[\tilde{\mathbf{H}}\right]_{p,q} = \tilde{h_{p,q}}$, we assume that

$$\begin{aligned}
\mathbb{E}\left\{\tilde{h}^R_{p,q}\tilde{h}^R_{\hat{p},\hat{q}}\right\} &= \mathbb{E}\left\{\tilde{h}^I_{p,q}\tilde{h}^I_{\hat{p},\hat{q}}\right\}, \\
\mathbb{E}\left\{\tilde{h}^R_{p,q}\tilde{h}^I_{\hat{p},\hat{q}}\right\} &= \mathbb{E}\left\{\tilde{h}^I_{p,q}\tilde{h}^R_{\hat{p},\hat{q}}\right\} = 0,
\end{aligned}$$

where $p, \hat{p} \in \{1, \ldots, N_r\}$ and $q, \hat{q} \in \{1, \ldots, N_t\}$. Explicitly, for each $\tilde{h}_{p,q}$, the auto-correlations of the real and imaginary parts are identical and the cross-correlations between real and imaginary parts are equal to zero. Hence, the correlated channel matrix can be described by the widely used Kronecker correlation model [53], which is expressed as

$$\tilde{\mathbf{H}} = \mathbf{\Sigma}_r^{\frac{1}{2}}\hat{\mathbf{H}}\mathbf{\Sigma}_t^{\frac{1}{2}}.$$

Here, $\mathbf{\Sigma}_t \in \mathbb{C}^{N_t \times N_t}$ and $\mathbf{\Sigma}_r \in \mathbb{C}^{N_r \times N_r}$ are the correlation matrices at V_1 and V_2, respectively, with the elements defined as $[\mathbf{\Sigma}_t]_{q,\hat{q}} = \sigma^t_{q,\hat{q}}$ for $q, \hat{q} \in \{1, \ldots, N_t\}$, and $[\mathbf{\Sigma}_r]_{p,\hat{p}} = \sigma^r_{p,\hat{p}}$ for $p, \hat{p} \in \{1, \ldots, N_r\}$. Furthermore, $\hat{\mathbf{H}}$ is the independent Rayleigh channel matrix whose entries are i.i.d complex Gaussian random variables, i.e. $[\hat{\mathbf{H}}]_{p,q} = \hat{h}_{p,q} \sim \mathscr{CN}(0, 1)$. Specifically, the correlation matrices $\mathbf{\Sigma}_t$ and $\mathbf{\Sigma}_r$ can be determined according to a concrete model. Here, the exponential model of Loyka [54] is adopted, and the correlation matrix entries are formed as $\sigma^t_{q,\hat{q}} = \kappa_t^{|q-\hat{q}|}$ and $\sigma^r_{p,\hat{p}} = \kappa_r^{|p-\hat{p}|}$, where κ_t and κ_r are the adjacent antenna correlation coefficients at V_1 and V_2, respectively.

In order to mimic the influence of the V2V channel's time-varying effects, we take the temporal correlation into consideration, which is defined as

$$\delta(\tau) = \mathbb{E}\left\{\hat{\mathbf{H}}(t)\,\hat{\mathbf{H}}(t+\tau)\right\},$$

where τ is the sampling time. In [43], Jakes' model is used for describing the temporal correlation expressed as $\delta(\tau) = J_0(2\pi f_D \tau)$, where f_D is the maximum Doppler frequency related to both the carrier frequency and the velocity of the terminal. For simplicity of analysis, in the following, we omit the index τ. Observe that $\delta = 1$ indicates that the underlying V2V channel is quasi-static, while $\delta < 1$ is related to a time-varying channel due to mobility. Naturally, both the spatial and temporal correlations would affect the performance of the receivers.

11.3 Capacity Analysis of the NOMA-SM System

Recall that the proposed NOMA-SM transmission scheme relies on a pair of independent spaces: the classical signal-domain, pertaining to the radiated superimposed symbol $\sqrt{\alpha}\gamma_l + \sqrt{1-\alpha}\chi_m$, and the Tx-domain, pertaining to the activated Tx index n_t. More specifically, the message intended for V_2 is conveyed by both of the two streams. While the message destined for U is only mapped to the classical signal-domain, superimposed with part of V_2's signal in the power domain. In what follows, we investigate the capacity of the collaboration-aided vehicle V_2 and the in-car user U. Monte Carlo estimates are also provided for MI evaluation, followed by an illustrative example to augment the theoretical analysis.

11.3.1 Capacity Analysis of the Collaboration-Aided Vehicle

In the NOMA protocol, the transmit power assigned by V_1 to the distant user V_2 has to be higher than that to the close-by user U. Then, the distant user directly detects its signal, since the interference induced by the close-by user is lower and can thus be treated as background noise. Considering that all Txs of V_1 are activated with the same probability for NOMA-SM, the instantaneous capacity pertaining to the classical signal-domain of V2V transmission is given by

$$\begin{aligned} C_V^{sig} &= \max_{f_\chi} I(\chi; \mathbf{y}_V | n_t) \\ &= \frac{1}{N_t} \sum_{i=1}^{N_t} \log_2\left(\frac{E_s p_0 \|\mathbf{h}_i\|^2 + \sigma_0^2}{\alpha E_s p_0 \|\mathbf{h}_i\|^2 + \sigma_0^2}\right). \end{aligned} \tag{11.5}$$

Observe that no practical modulation constellation is assumed, when performing these capacity calculations. Since the channel capacity relates to the highest rate in

bits per channel use at which information can be sent with arbitrarily low probability of error, in (11.5), we substitute χ_m by χ, which denotes a random input signal alphabet with a distribution of f_χ. On the other hand, the MI conveyed by the spatial-domain Tx-constellations can be written as

$$I\left(n_t; \mathbf{y}_V\right) = \frac{1}{N_t} \sum_{i=1}^{N_t} \int \Pr\left(\mathbf{y}_V | \mathbf{h}_i\right) \log_2 \frac{\Pr\left(\mathbf{y}_V | \mathbf{h}_i\right)}{\Pr\left(\mathbf{y}_V\right)} \mathrm{d}\mathbf{y}_V, \tag{11.6}$$

where $\Pr\left(\mathbf{y}_V | \mathbf{h}_i\right)$ denotes the probability density function (PDF) of the channel output $\mathbf{y}_V$ received over the ith channel vector of $\mathbf{H}$, given by

$$\Pr\left(\mathbf{y}_V | \mathbf{h}_i\right) = \frac{1}{\pi^{N_r} \det\left(\mathbf{\Sigma}_i\right)} \exp\left\{-\mathbf{y}_V^H \mathbf{\Sigma}_i^{-1} \mathbf{y}_V\right\},$$

where $\mathbf{\Sigma}_i = \sigma_0^2 \mathbf{I} + p E_s \mathbf{h}_i \mathbf{h}_i{}^H$. As a result, the instantaneous capacity of V_2 in the NOMA-SM system is formulated as

$$C_V = C_V^{sig} + I\left(n_t; \mathbf{y}_V\right). \tag{11.7}$$

Remark It is worth noting that in (11.5), C_V^{sig} is achievable where the optimum input distribution for χ is Gaussian. In fact, this optimum input distribution is also regarded as the optimum input distribution for a conventional SM system. This is a common assumption in the majority of SM capacity-related contributions [28, 55–57], effectively simplifying the analysis. Nevertheless, a fundamental weakness of the Gaussian input assumption is that f_χ affects both $I\left(\chi; \mathbf{y}_V | n_t\right)$ and $I\left(n_t; \mathbf{y}_V\right)$. Clearly, the Gaussian input distribution maximizes $I\left(\chi; \mathbf{y}_V | n_t\right)$, but it is unclear whether it maximizes $I\left(n_t; \mathbf{y}_V\right)$. In addition, the equiprobable activation of antennas is a widely accepted assumption for SM-enabled systems, albeit this activation regime cannot guarantee the optimal spatial design capable of achieving the capacity in the Tx-domain. Actually, Liu et al. in [55] studied the optimal antenna activation required for Tx-domain capacity maximization. Moreover, Basnayaka et al. [30] have demonstrated that the Gaussian input does not achieve the upper limit of the MI provided by an SM-aided system. As a further insight, although the MI conveyed by the Tx-domain cannot be formulated as an analytical expression, we are inspired to derive the capacity upper bound and to conceive the associated power allocation optimization schemes, which will be addressed in Sect. 11.5.

11.3.2 Capacity Analysis of the In-Car User

In contrast to the receiver of V_2, the receiver of U can detect its own signal after removing the interference imposed by V_2, as seen in Fig. 11.2. To demonstrate the feasibility of this SIC procedure, we first deduce the maximum rate of which U can

detect the message of V_2. Specifically, the maximum rate for U detecting the message related to the classical signal-domain of V_2 is given by

$$C_U^{V,sig} = \frac{1}{N_t} \sum_{i=1}^{N_t} \log_2 \left(\frac{E_s \|\mathbf{g}_i\|^2 + \sigma_0^2}{\alpha E_s \|\mathbf{g}_i\|^2 + \sigma_0^2} \right). \tag{11.8}$$

The MI associated with U detecting the information embedded in the Tx-constellation of V_2 can be written as

$$I\left(n_t; \mathbf{y}_U\right) = \frac{1}{N_t} \sum_{i=1}^{N_t} \int \Pr\left(\mathbf{y}_U \,|\, \mathbf{g}_i\right) \log_2 \frac{\Pr\left(\mathbf{y}_U \,|\, \mathbf{g}_i\right)}{\Pr\left(\mathbf{y}_U\right)} \mathrm{d}\mathbf{y}_U, \tag{11.9}$$

where $\Pr\left(\mathbf{y}_U \,|\mathbf{g}_i\right)$ denotes the PDF of the channel output $\mathbf{y}_U$ received over the ith channel vector of $\mathbf{G}$ given by

$$\Pr\left(\mathbf{y}_U \,|\mathbf{g}_i\right) = \frac{1}{\pi^{N_u} \det\left(\mathbf{\Omega}_i\right)} \exp\left\{-\mathbf{y}_U^H \mathbf{\Omega}_i^{-1} \mathbf{y}_U\right\},$$

where $\mathbf{\Omega}_i = \sigma_0^2 \mathbf{I} + E_s \mathbf{g}_i \mathbf{g}_i{}^H$. As a result, the instantaneous capacity for U detecting the signal of V_2 can be expressed as

$$C_U^V = C_U^{V,sig} + I\left(n_t; \mathbf{y}_U\right). \tag{11.10}$$

It may be readily seen that $C_U^V > C_V$ is always satisfied, since $\|\mathbf{g}_i\|^2 > p_0 \|\mathbf{h}_i\|^2$, guaranteeing the success of SIC. Hence, the capacity of U detecting its own desired signal is written as

$$\begin{aligned} C_U &= \max_{f_\gamma} I\left(\gamma; \mathbf{y}_U \,|\, n_t, \chi, \mathbf{G}\right) \\ &= \tfrac{1}{N_t} \sum_{i=1}^{N_t} \log_2 \left(1 + \tfrac{\alpha E_s}{\sigma_0^2} \|\mathbf{g}_i\|^2\right), \end{aligned} \tag{11.11}$$

where γ denotes the random input signal variable related to the desired message of U, with a distribution of f_γ. The capacity for U detecting γ indeed becomes achievable when the channel's input distribution f_γ is Gaussian.

11.3.3 Mutual Information

To appreciate the above theoretical analysis in terms of its relevance, next, we characterize the bandwidth efficiency of the proposed NOMA-SM. Assuming perfect knowledge of the instantaneous channel state information at both receivers, the MI achieved by V_2 and U with the aid of practical APM constellations is evaluated by the classical Monte Carlo method. For the collaboration-aided vehicle V_2, the MI

between a discrete signal input (n_t, χ_m) and the received signal $\mathbf{y}_V$ can be formulated as

$$\begin{aligned} I(n_t, \chi_m; \mathbf{y}_V | \mathbf{H}) &= \mathbb{E}_{n_t,\chi_m,\mathbf{y}_V}\left\{\log_2 \frac{\Pr(\mathbf{y}_V|n_t,\chi_m,\mathbf{H})}{\Pr(\mathbf{y}_V|\mathbf{H})}\right\} \\ &= \frac{1}{N_t M} \times \int \Pr(\mathbf{y}_V | \chi_m, \mathbf{h}_i) \log_2 \frac{\Pr(\mathbf{y}_V|\chi_m,\mathbf{h}_i)}{\Pr(\mathbf{y}_V|\mathbf{H})} d\mathbf{y}_V, \end{aligned} \tag{11.12}$$

where the conditional probability $\Pr(\mathbf{y}_V | \chi_m, \mathbf{h}_i)$ is expressed as

$$\begin{aligned} \Pr(\mathbf{y}_V | \chi_m, \mathbf{h}_i) = &\frac{1}{\pi^{N_r} \det(\Psi_i)} \exp\Big\{-\big(\mathbf{y}_V - \sqrt{p_0(1-\alpha)}\mathbf{h}_i \chi_m\big)^H \\ &\times \mathbf{\Psi}_i^{-1}\big(\mathbf{y}_V - \sqrt{p_0(1-\alpha)}\mathbf{h}_i \chi_m\big)\Big\}, \end{aligned}$$

with $\mathbf{\Psi}_i = \sigma_0^2 \mathbf{I} + \alpha p_0 E_s \mathbf{h}_i \mathbf{h}_i^H$. With regard to the in-car user U performing SIC first, the MI between the information input (n_t, χ_m) and the received signal $\mathbf{y}_U$ is given by

$$\begin{aligned} I(n_t, \chi_m; \mathbf{y}_U | \mathbf{G}) = &\frac{1}{N_t M} \times \\ &\int \Pr(\mathbf{y}_U | \chi_m, \mathbf{g}_i) \log_2 \frac{\Pr(\mathbf{y}_U|\chi_m,\mathbf{g}_i)}{\Pr(\mathbf{y}_U|\mathbf{G})} d\mathbf{y}_U, \end{aligned} \tag{11.13}$$

where the conditional probability $\Pr(\mathbf{y}_U | \chi_m, \mathbf{g}_i)$ is expressed as

$$\begin{aligned} &\Pr(\mathbf{y}_U | \chi_m, \mathbf{g}_i) = \frac{1}{\pi^{N_u} \det(\mathbf{\Phi}_i)} \times \\ &\exp\Big\{-\big(\mathbf{y}_U - \sqrt{1-\alpha}\mathbf{g}_i \chi_m\big)^H \mathbf{\Phi}_i^{-1}\big(\mathbf{y}_U - \sqrt{1-\alpha}\mathbf{g}_i \chi_m\big)\Big\}, \end{aligned}$$

with $\mathbf{\Phi}_i = \sigma_0^2 \mathbf{I} + \alpha E_s \mathbf{g}_i \mathbf{g}_i^H$.

Subsequently, the MI between the information input γ_l and the received signal $\mathbf{y}_U$ after perfect SIC is expressed as

$$I\left(\gamma_l; \tilde{\mathbf{y}}_U | \mathbf{g}_{n_t}\right) = \frac{1}{N_t L} \int \Pr(\tilde{\mathbf{y}}_U | \gamma_l, \mathbf{g}_i) \log_2 \frac{\Pr(\tilde{\mathbf{y}}_U|\gamma_l,\mathbf{g}_i)}{\frac{1}{N_t L}\sum_{k,j} \Pr\left(\tilde{\mathbf{y}}_U|\gamma_k,\mathbf{g}_j\right)} d\tilde{\mathbf{y}}_U, \tag{11.14}$$

where $\tilde{\mathbf{y}}_U = \mathbf{y}_U - \sqrt{1-\alpha}\mathbf{g}_i \chi_m$ with $i \in \{1, \ldots, N_t\}$ and $m \in \{1, \ldots, M\}$ denotes the received vector after SIC. The conditional probability $\Pr(\tilde{\mathbf{y}}_U | \gamma_l, \mathbf{g}_i)$ is given by

$$\Pr(\tilde{\mathbf{y}}_U | \gamma_l, \mathbf{g}_i) = \frac{1}{\left(\pi\sigma_0^2\right)^{N_u}} \exp\left\{-\frac{\left\|\tilde{\mathbf{y}}_U - \sqrt{\alpha}\mathbf{g}_i \gamma_l\right\|^2}{\sigma_0^2}\right\}.$$

11.3.4 An Illustration

In this part, a simulation-based study of our theoretical expressions is provided with the aid of the MI attained by practical APM constellations. We set $N_t = 64$, $N_r = N_u = 2$ for our MIMO configurations in conjunction with $\alpha = 0.1$, $E_s = 1$ and $p_0 = 10^{-3}$ are given. The channel matrix $\mathbf{H}$ is generated according to Sect. 11.2.2, where $K = 0.2, \kappa_t = \kappa_r = 0.5$, and $\delta = 1$ are used. Each entry of $\mathbf{G}$ is identically and independently generated according to a complex Gaussian distribution $\mathcal{CN}(0, 1)$. In our Monte Carlo evaluations, the 16PSK signal constellation is chosen as the APM for χ_m and γ_l; hence, we have $M = L = 16$. The effective transmit signal-to-noise ratio (SNR) at V_1 is given by $p_0 E_s/\sigma_0^2$ as the horizontal axis of Fig. 11.3. Notice that the transmit-SNR cannot be readily interpreted physically, because it relates the transmitter power to the noise power at the receiver, but its notion is convenient to use in NOMA-aided scenarios. Given the effective transmit-SNR at V_1 as $\text{SNR} = p_0 E_s/\sigma_0^2$, the average receive-SNR at V_2 can be computed as

$$\text{SNR}_r^{V_2} = \frac{(1-\alpha)\,\text{SNR}}{1+\alpha\text{SNR}}.$$

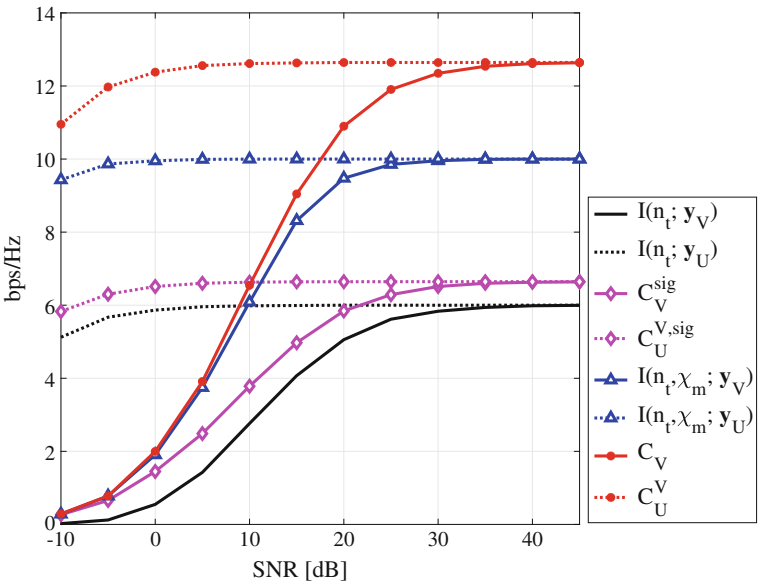

Fig. 11.3 Capacity and MI performance for $N_t = 64$, $N_r = N_u = 2$, $M = L = 16$, and $\alpha = 0.01$. Specifically, C_V^{sig}, $C_U^{V,sig}$, $I(n_t; \mathbf{y}_V)$, and $I(n_t; \mathbf{y}_U)$ are obtained from (11.5), (11.8), (11.6), and (11.9), respectively. While $I(n_t, \chi_m; \mathbf{y}_V)$ and $I(n_t, \chi_m; \mathbf{y}_U)$ are generated from (11.12) and (11.13), respectively, after averaging over multiple channel realizations. Finally, C_V and C_U^V are evaluated from (11.7) and (11.10), respectively

Similarly, the average receive-SNR at U for detecting the signal of V_2 and that of itself is respectively expressed as

$$\mathrm{SNR}_r^{U,V_2} = \frac{(1-\alpha)\mathrm{SNR}}{p_0+\alpha\mathrm{SNR}},$$
$$\mathrm{SNR}_r^{U} = \frac{\alpha\mathrm{SNR}}{p_0}.$$

Hence, the effective transmit-SNR at V_1 is unambiguously related to the SNRs at each receiver. Furthermore, we use $\mathrm{SNR} = p_0 E_s/\sigma_0^2$ in all of the subsequent performance analyses.

The relevant results of Fig. 11.3 are discussed as follows.

- The capacity of V_2 gleaned from the signal-domain, that is C_V^{sig} obtained from (11.5), increases steadily up to a saturation point as the SNR increases. By contrast, the capacity for U detecting the signal-domain destined for V_2, i.e. $C_U^{V,sig}$ obtained from (11.8), is higher than C_V^{sig} in the low and moderate SNR domain. Clearly, a successful detection of the signal-domain of V_2 can be performed by U.
- The MI $I(n_t; \mathbf{y}_V)$ generated using (11.6) increases with the SNR and saturates at 6 bps/Hz, since the input entropy of the Tx-domain space is $\log_2(N_t)$. By contrast, the MI $I(n_t; \mathbf{y}_U)$ attained by (11.9) is as high as 6 bps/Hz across almost the entire SNR range, since the channel quality of U is much higher than that of V_2, implying that U can successfully detect the signal of V_2 embedded in the Tx-domain.
- The capacity of V_2, i.e. C_V, grows steadily as the SNR increases up to its saturation at high SNRs, but it remains lower than C_U^V. Since C_V is obtained by the summation of C_V^{sig} and $I(n_t; \mathbf{y}_V)$, and C_U^V equals to the sum of $C_U^{V,sig}$ and $I(n_t; \mathbf{y}_U)$. Naturally, $C_U^V > C_V$ is satisfied, as $C_U^{V,sig}$ and $I(n_t; \mathbf{y}_U)$ are higher than C_V^{sig} and $I(n_t; \mathbf{y}_V)$, respectively. Therefore, U can always perform successful SIC.
- The MI curves $I(n_t, \chi_m; \mathbf{y}_V)$ and $I(n_t, \chi_m; \mathbf{y}_U)$ are generated from (11.12) and (11.13), respectively, after averaging over multiple channel realizations. It may be observed that the simulated curve $I(n_t, \chi_m; \mathbf{y}_V)$ matches the analytical capacity C_V quite closely upto an SNR of 5 dB, but beyond that $I(n_t, \chi_m; \mathbf{y}_V)$ starts to drift away from C_V. By contrast, the drift of $I(n_t, \chi_m; \mathbf{y}_U)$ from C_U^V remains nearly unchanged. Both drifts are due to the fact that the MI attained with the aid of practical APM modulation is upper bounded by the capacity, namely by the maximum data rate related to the optimal input distribution.

11.4 Power Allocation Algorithms

It has been demonstrated that the MI conveyed by the Tx-domain cannot be readily formulated as a closed-form expression, only by resorting to simulations. Thus, it is very hard to perform an optimal power allocation for NOMA-SM. To circumvent this problem, we first derive an upper bound of the NOMA-SM capacity. Then the power allocation, which is capable of maximizing the capacity bound is considered, leading to the optimal solution.

11.4.1 Problem Formulation

Theoretically, the instantaneous capacity of V_2 in the NOMA-SM system can be expressed as

$$C_V = \max_{f_\chi} I\left(n_t, \chi; \mathbf{y}_V\right) = \max_{f_\chi} h\left(\mathbf{y}_V\right) - h\left(\mathbf{y}_V \left| n_t, \chi \right.\right), \tag{11.15}$$

where $h(\cdot)$ denotes the differential entropy. The conditional differential entropy $h\left(\mathbf{y}_V \left| n_t, \chi \right.\right)$ in (11.15) is explicitly given by

$$h\left(\mathbf{y}_V \left| n_t, \chi \right.\right) = \frac{1}{N_t} \sum_{i=1}^{N_t} \log_2 \det\left[\pi e \left(p_0 \alpha E_s \mathbf{h}_i \mathbf{h}_i^H + \sigma_0^2 \mathbf{I}\right)\right].$$

To determine C_V, we have to evaluate $h\left(\mathbf{y}_V\right)$, which requires the knowledge of the distribution of $\mathbf{y}_V$. It may be readily seen that the MI $I\left(n_t, \chi; \mathbf{y}_V\right)$ is maximized if the vector variable $\mathbf{y}_V$ has a Gaussian distribution. Thus, we assume that the received vector $\mathbf{y}_V$ has a Gaussian distribution, which is a zero-mean vector having a covariance matrix presented as

$$\begin{aligned}
\mathbb{E}\left\{\mathbf{y}_V \mathbf{y}_V^H\right\} &= \mathbf{H}\mathbb{E}_{n_t}\left\{\mathbf{e}_{n_t}\mathbb{E}_\chi\left\{p_0\left(1-\alpha\right)\chi\chi^*\right\}\mathbf{e}_{n_t}^H\right\}\mathbf{H}^H \\
&\quad + \mathbf{H}\mathbb{E}_{n_t}\left\{\mathbf{e}_{n_t}\mathbb{E}_\gamma\left\{p_0\alpha\gamma\gamma^*\right\}\mathbf{e}_{n_t}^H\right\}\mathbf{H}^H + \sigma_0^2\mathbf{I} \\
&= \mathbf{H}\left\{\frac{1}{N_t}\sum_{i=1}^{N_t}\mathbf{e}_i\mathbf{e}_i^H p_0\left(1-\alpha\right)E_s\right\}\mathbf{H}^H \\
&\quad + \mathbf{H}\left\{\frac{1}{N_t}\sum_{n_t=1}^{N_t}\mathbf{e}_i\mathbf{e}_i^H p_0\alpha E_s\right\}\mathbf{H}^H + \sigma_0^2\mathbf{I} \\
&= \frac{p_0 E_s}{N_t}\mathbf{H}\mathbf{H}^H + \sigma_0^2\mathbf{I}.
\end{aligned}$$

An upper bound of $h\left(\mathbf{y}_V\right)$ can be formulated as

$$h\left(\mathbf{y}_V\right) \le \log_2 \det\left(\pi e\left(\frac{p_0 E_s}{N_t}\mathbf{H}\mathbf{H}^H + \sigma_0^2\mathbf{I}\right)\right).$$

Hence, we obtain an upper bound of C_V which is written as

$$\begin{aligned} C_V &\leq \log_2 \det\left(\pi e\left(\tfrac{p_0 E_s}{N_t}\mathbf{H}\mathbf{H}^H + \sigma_0^2\mathbf{I}\right)\right) \\ &\quad -\tfrac{1}{N_t}\sum_{i=1}^{N_t}\log_2 \det\left(\pi e\left(p_0\alpha E_s \mathbf{h}_i\mathbf{h}_i^H + \sigma_0^2\mathbf{I}\right)\right) \\ &= \sum_{j=1}^{N_r}\log_2\left(\tfrac{p_0 E_s}{N_t}\lambda_j^2 + \sigma_0^2\right) \\ &\quad -\tfrac{1}{N_t}\sum_{i=1}^{N_t}\log_2\left(p_0\alpha E_s\|\mathbf{h}_i\|^2 + \sigma_0^2\right) \triangleq C_V^{B_1}, \end{aligned} \tag{11.16}$$

where λ_j is the jth singular value of $\mathbf{H}$ with $j \in \{1, \ldots, N_r\}$. Clearly, $C_V^{B_1}$ has N_r DoFs, and it is the same as the capacity of an $(N_t \times N_r)$-element spatially multiplexed MIMO system, subject to inter-user interference.

On the other hand, the MI of the Tx-domain has a natural upper bound written as

$$I\left(n_t; \mathbf{y}_V\right) \leq \log_2\left(N_t\right),$$

which corresponds to the maximum MI that can be conveyed by the Tx-domain of the V2V transmission link. Now, another upper bound of C_V may also be formulated as

$$\begin{aligned} C_V &\leq C_V^{sig} + \log_2\left(N_t\right) \\ &= \tfrac{1}{N_t}\sum_{i=1}^{N_t}\log_2\left(\tfrac{E_s p_0\|\mathbf{h}_i\|^2+\sigma_0^2}{\alpha E_s p_0\|\mathbf{h}_i\|^2+\sigma_0^2}\right) + \log_2\left(N_t\right) \triangleq C_V^{B_2}. \end{aligned} \tag{11.17}$$

Before proceeding, we provide a numerical illustration in order to evaluate both of the upper bounds on the capacity of V_2. Figure 11.4 depicts C_V and both upper bounds of the NOMA-SM system in conjunction with $N_t = 64, N_r = 2, M = 16$, and $\alpha = 0.1$, which exhibit distinct approximations of C_V within certain SNR regions. The upper bound $C_V^{B_1}$ gives a tight bound of C_V at low SNRs, indicating that the NOMA-SM capacity at V_2 is almost the same as that of a spatially multiplexed MIMO system of the same configuration in the presence of inter-user interference. However, the MI embedded in the Tx-domain saturates as the SNR increases, which is due to the fact that N_t is finite. Hence, at high SNRs, $C_V^{B_2}$ is much tighter.

Based on the above observations, a refined upper bound on the capacity of V_2 in the NOMA-SM system is represented as

$$C_V^B \triangleq \min\left(C_V^{B_1}, C_V^{B_2}\right). \tag{11.18}$$

Considering the QoS of the two receivers from a practical perspective, we define the minimum rate requirement of V_2 and U as $\tilde{C}_V$ and $\tilde{C}_U$, respectively. The optimization problem constructed for maximizing the sum capacity with a power allocation factor of α can be formulated as

$$\mathscr{P}: \max_{\alpha} C_U + C_V^B$$

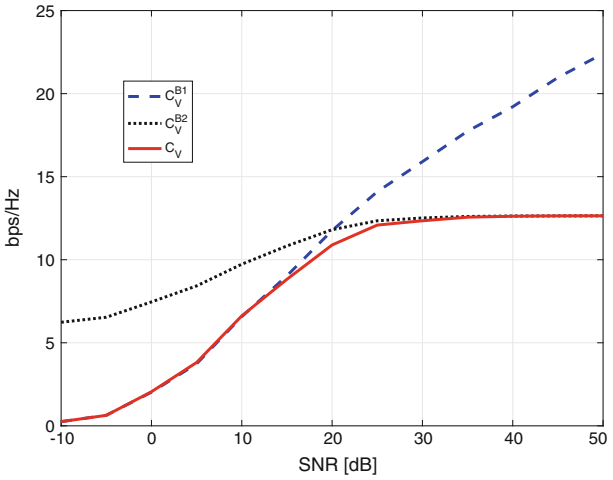

Fig. 11.4 Capacity and two upper bounds of the V2V transmission link with $N_t = 64$, $N_r = 2$, $M = 16$, and $\alpha = 0.01$. Specifically, C_V, $C_V^{B_1}$, and $C_V^{B_2}$ are evaluated from (11.7), (11.16), and (11.17), respectively

$$s.t. \begin{cases} C_U \geq \tilde{C}_U, & (a) \\ C_V^B \geq \tilde{C}_V, & (b) \\ 0 < \alpha < \frac{1}{2}. & (c) \end{cases} \tag{11.19}$$

11.4.2 The Proposed Power Allocation Algorithm

To solve the proposed optimization problem, we first express the derivatives of C_U, $C_V^{B_1}$, and $C_V^{B_2}$ with respect to α as

$$\begin{aligned} \frac{\mathrm{d}C_U}{\mathrm{d}\alpha} &= \frac{1}{N_t} \sum_{i=1}^{N_t} \frac{E_s \|\mathbf{g}_i\|^2}{\alpha E_s \|\mathbf{g}_i\|^2 + \sigma_0^2}, \\ \frac{\mathrm{d}C_V^{B_1}}{\mathrm{d}\alpha} &= -\frac{1}{N_t} \sum_{n_t=1}^{N_t} \frac{E_s p_0 \|\mathbf{h}_i\|^2}{\alpha E_s p_0 \|\mathbf{h}_i\|^2 + \sigma_0^2}, \\ \frac{\mathrm{d}C_V^{B_2}}{\mathrm{d}\alpha} &= -\frac{1}{N_t} \sum_{n_t=1}^{N_t} \frac{E_s p_0 \|\mathbf{h}_i\|^2}{\alpha E_s p_0 \|\mathbf{h}_i\|^2 + \sigma_0^2}, \end{aligned} \tag{11.20}$$

respectively. Observe from (11.20) that C_U is a monotonically increasing function of α, given its positive derivative, while both $C_V^{B_1}$ and $C_V^{B_2}$ are decreasing ones. Thus, when the constraint (c) of (11.19) is taken into account, there exist both minimum

and maximum capacities that V_2 and U can achieve. Furthermore, to satisfy the constraint (a) and (b), we have the following conditions for $\tilde{C}_U$ and $\tilde{C}_V$, respectively

$$0 < \tilde{C}_U < C_U\left(\alpha = \frac{1}{2}\right),$$

$$C_V^B\left(\alpha = \frac{1}{2}\right) < \tilde{C}_V < C_V^B\left(\alpha = 0\right).$$

Given the above conditions, we can rewrite the constraints of problem $\mathscr{P}$ in a compact form as

$$g^{-1}\left(\tilde{C}_U\right) < \alpha < f^{-1}\left(\tilde{C}_V\right),$$

where $g^{-1}(\cdot)$ and $f^{-1}(\cdot)$ indicate the inverse function of C_U and C_V^B, respectively. To guarantee that the feasible set of problem $\mathscr{P}$ is non-empty, a further refined condition for setting $\tilde{C}_V$ is given by

$$C_V^B\left(\alpha = \frac{1}{2}\right) < \tilde{C}_V < C_V^B\left[\alpha = g^{-1}\left(\tilde{C}_U\right)\right].$$

Moreover, since $\left\|\mathbf{g}_{n_t}\right\|^2 > p_0\left\|\mathbf{h}_{n_t}\right\|^2$ is always satisfied, the derivative of $\left(C_U + C_V^B\right)$ can be guaranteed to have a positive value. Accordingly, the objective function of problem $\mathscr{P}$ is a monotonically increasing function and can be maximized, when α reaches the upper bound of its feasible set. With $\tilde{C}_U$ and $\tilde{C}_V$ being appropriately set, we find that the upper bound of α's feasible set is related to the constraint (b) of (11.19), and the lower bound corresponds to the constraint (a) of (11.19). Thus, the optimal solution of problem $\mathscr{P}$ is

$$\alpha_{opt}^{\mathscr{P}} = f^{-1}\left(\tilde{C}_V\right). \tag{11.21}$$

This optimal solution implies that the amount of power allocated to V_2 is 'just' sufficient to meet the minimum rate requirement $\tilde{C}_V$, while the remaining power is used for U, aiming for maximizing its capacity. Nevertheless, we should notice that there may exist some practical considerations, which require us to give high priority to the V2V transmission link, such as those of safety applications, which have to be served reliably. By contrast, the transmissions for in-car users are typically related to infotainment applications, for example peer-to-peer video sharing and multimedia advertisements [58]. Hence, it may be desirable to maximize the data rate of the V2V link, while guaranteeing the minimum rate requirement of the in-car user. To this end, we develop an alternative optimization problem formulated as

$$\mathscr{O}: \max_{\alpha} C_V^B$$

$$s.t. \begin{cases} C_U \geq \tilde{C}_U, & (a) \\ C_V^B \geq \tilde{C}_V, & (b) \\ 0 < \alpha < \frac{1}{2}. & (c) \end{cases} \tag{11.22}$$

Clearly, the objective function of (11.22) is a monotonically decreasing function of α, and it is maximized, when the constraint (a) is inactive. Therefore, the optimal solution of problem $\mathscr{O}$ can be written as

$$\alpha_{opt}^{\mathscr{O}} = g^{-1}\left(\tilde{C}_U\right). \tag{11.23}$$

So far, we have proposed a pair of power allocation schemes and analysed the solvability of the optimization problems considered. Explicitly, we provided an algorithm for finding the optimal solution of each problem, which are summarized in Table 11.1. The proposed algorithm essentially performs bounding through with the aid of a bisection procedure, yielding globally optimal solutions at linearly increasing computational complexity [59]. In specific, the minimum rate requirements of V_2 and U are respectively set as

$$\begin{aligned} \tilde{C}_U &= \frac{C_U\left(\alpha = \frac{1}{2}\right)}{2}, \\ \tilde{C}_V &= \frac{C_V^B\left(\alpha = \frac{1}{2}\right) + C_V^B\left[\alpha = g^{-1}\left(\tilde{C}_U\right)\right]}{2}, \end{aligned} \tag{11.24}$$

for simplicity. Basically, both of the two power allocation optimization problems satisfy realistic practical considerations, and the suitable one can be flexibly selected based on the specific data priority of the distinct transmission links.

11.5 Simulations and Discussions

In this section, simulation results are provided for evaluating the performance of the proposed NOMA-SM scheme. The system parameters are summarized as follows. The MIMO configurations for the NOMA-SM system are set as $N_t = 64$, $N_r = N_u = 2$. We fix $p_0 = 10^{-3}$, or, equivalently, the path loss exponential is set to 3, and the distance between V_1 and V_2 is assumed to be 10 m, which is typical for urban environments, especially during rush hours.

Table 11.1 Power Allocation Algorithm

Power Allocation Algorithm for Problem $\mathscr{P}$ and Problem $\mathscr{O}$

1. Initialization

Set tolerance $0 < \varepsilon \ll 1$. Calculate $C_U\left(\alpha = \frac{1}{2}\right)$ and set $\tilde{C}_U = C_U\left(\alpha = \frac{1}{2}\right)/2$.

2. Determine the lower bound of α and find the optimal solution of problem $\mathscr{O}$

Set $\alpha_L = 0$ and $\alpha_U = \frac{1}{2}$.
While $\alpha_L - \alpha_U > \varepsilon$
  Set $\alpha = \frac{\alpha_L + \alpha_U}{2}$. Calculate $C_U(\alpha)$.
  If $C_U(\alpha) - \tilde{C}_U > 0$
    $\alpha_U = \alpha$
  Else
    $\alpha_L = \alpha$.
  End
End
Set $\tilde{C}_V = \left[C_V^B\left(\alpha = \frac{1}{2}\right) + C_V^B\left(\alpha = \frac{\alpha_L + \alpha_U}{2}\right)\right]/2$.
The optimal solution to the problem $\mathscr{O}$ is obtained as $\alpha_{opt}^{\mathscr{O}} = \frac{\alpha_L + \alpha_U}{2}$. Calculate $C_U\left(\alpha_{opt}^{\mathscr{O}}\right)$ and $C_V^B\left(\alpha_{opt}^{\mathscr{O}}\right)$.

3. Determine the upper bound of α and find the optimal solution of problem $\mathscr{P}$

Set $\alpha_{\min} = \frac{\alpha_L + \alpha_U}{2}$ and $\alpha_{\max} = \frac{1}{2}$.
While $\alpha_{\max} - \alpha_{\min} > \varepsilon$
  Set $\alpha = \frac{\alpha_{\min} + \alpha_{\max}}{2}$. Calculate $C_V^B(\alpha)$.
  If $C_V^B(\alpha) - \tilde{C}_V > 0$
    $\alpha_{\min} = \alpha$
  Else
    $\alpha_{\max} = \alpha$.
  End
End
The optimal solution of the problem $\mathscr{P}$ is obtained as $\alpha_{opt}^{\mathscr{P}} = \frac{\alpha_{\min} + \alpha_{\max}}{2}$. Calculate $C_U\left(\alpha_{opt}^{\mathscr{P}}\right)$ and $C_V^B\left(\alpha_{opt}^{\mathscr{P}}\right)$.

11.5.1 BER Results and Discussions

In this subsection, the BER performance of the NOMA-SM scheme is compared to NOMA relying on the popular VBLAST technique, termed NOMA-VBLAST. Specifically, we focus on the receiver performance of V_2. The effects of the Rician K-factor, adjacent antenna correlation coefficient, temporal correlation, and power allocation factor are all taken into consideration. The Rician K-factors are configured as $K = 2.186$ and $K = 0.2$ for low and high vehicular traffic density, respectively (see [51] for more details). More specifically, we consider a pair of references: NOMA-VBLAST applied with 16QAM and $N_t = 2$, and NOMA-VBLAST adopted QPSK and $N_t = 4$. The MIMO configuration of the references is the same as that of NOMA-SM except for N_t. Besides, QPSK is applied for NOMA-SM. Thus, the following BER comparisons are carried out for the same bandwidth efficiency of 8 bits per channel use (bpcu). The optimum ML detector described in (11.4) is

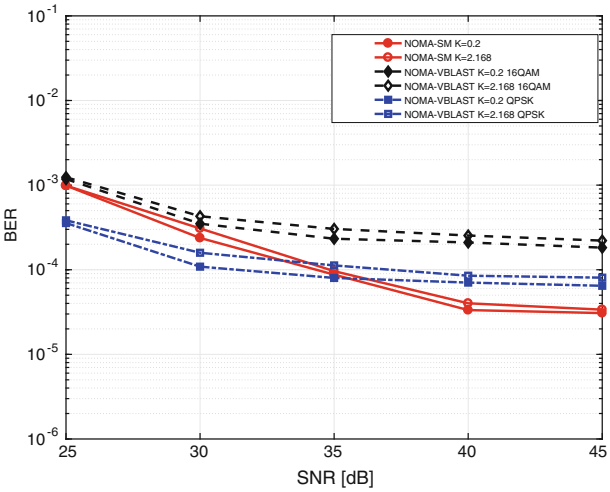

Fig. 11.5 BER comparisons with different Rician K-factor when $\kappa_t = \kappa_r = 0.2$ and $\delta = 1$ are given, and the power allocation factor is fixed at $\alpha = 0.001$, as evaluated by the Monte Carlo simulation with 10^6 channel realizations

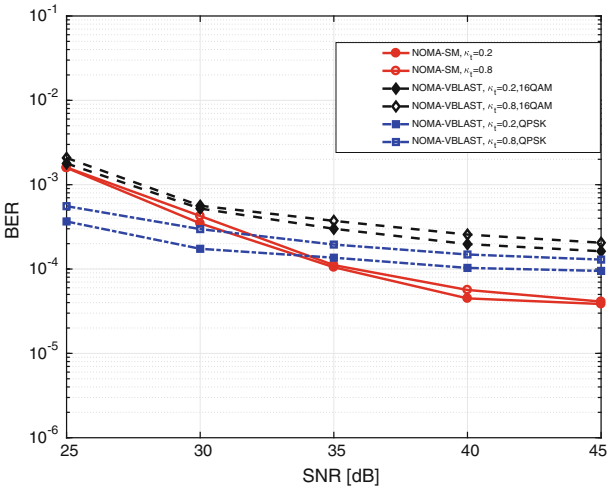

Fig. 11.6 BER comparisons with different adjacent antenna correlation coefficient at V_1, i.e. κ_t, when $K = 0.2$, $\kappa_r = 0.5$, and $\delta = 1$ are given, and the power allocation factor is fixed at $\alpha = 0.001$, as evaluated by the Monte Carlo simulation with 10^6 channel realizations

employed at V_2 in both schemes. All simulation results of this subsection are obtained through a Monte Carlo method.

In Fig. 11.5, we show the BER performance for different Rician K-factor. It is observed that NOMA-SM outperforms the benchmark especially in the high SNR regime. Additionally, the increase of K imposes a more dominant degradation on

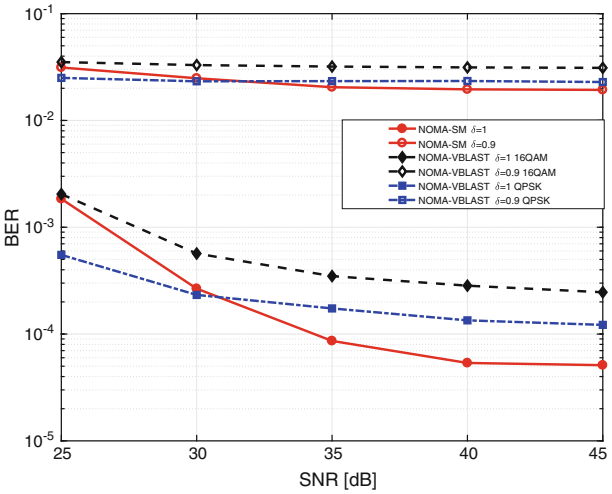

Fig. 11.7 BER comparisons with different temporal correlation coefficient δ when $K = 0.2$ and $\kappa_t = \kappa_r = 0.5$ are given, and the power allocation factor is fixed at $\alpha = 0.001$, as evaluated by the Monte Carlo simulation with 10^6 channel realizations

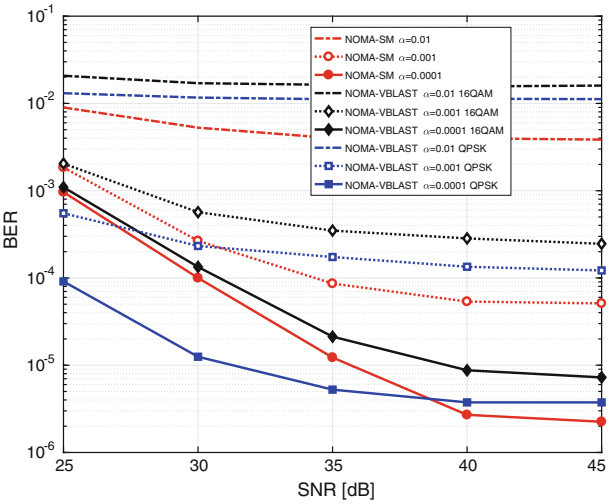

Fig. 11.8 BER comparisons with different power allocation factor α when $K = 0.2, \kappa_t = \kappa_r = 0.5$, and $\delta = 1$ are given, as evaluated by the Monte Carlo simulation with 10^6 channel realizations

both of the NOMA-VBLAST schemes, which rely more vitally on the presence of rich non-LoS scattering. This phenomenon can be explained as follows. The higher Rician factor K represents a stronger LoS component, which increases the spatial correlation among the adjacent channel paths. For NOMA-VBLAST schemes, the multiple-stream information is conveyed with the aid of multiple DoFs. By contrast, for NOMA-SM, although the more severe spatial correlation of the LoS scenario makes it difficult to determine the index of the activated Tx, the remaining information related to the APM signal-domain is transmitted over a single DoF; hence, it is less susceptible to spatial correlation.

Figure 11.6 investigates the BER results associated with different adjacent Tx-correlation coefficients at V_1. Compared to $\kappa_t = 0.8$, $\kappa_t = 0.2$ represents an insignificant spatial correlation. Again, observe from Fig. 11.6 that NOMA-SM is less susceptible to spatial correlation. This phenomenon can be interpreted similarly to the trend of Fig. 11.5. Besides, for these two figures, we notice that NOMA-SM temporarily loses its advantage over NOMA-VBLAST adopted QPSK and $N_t = 4$ within moderate SNR regime. This observation results from the superiority that QPSK brings to NOMA-VBLAST compared to 16QAM. However, as the increment of SNR, NOMA-SM achieves its dominance in terms of higher diversity gain.

Below, we investigate the impact of the V2V channel's time-varying nature. Observe from Fig. 11.7 that compared to the performance of no time-varying effect associated with $\delta = 1$, the BER has been substantially degraded in all schemes for $\delta = 0.9$. Although a perfect channel estimation procedure is assumed for the receivers, the estimated channel coefficients used for ML detection becomes partially outdated due to the channel's time-varying nature, hence resulting in a degraded BER performance. Nevertheless, the proposed NOMA-SM scheme maintains its advantage over the reference within the medium and high SNR regime, regardless of the grade of temporal correlation.

Figure 11.8 shows the BER performance associated with different α values. For all schemes, the lower α values exhibit a better detection performance, since less power is allocated to U and hence V_2 suffers from a lower inter-user interference. More importantly, we observe that NOMA-SM consistently outperforms the NOMA-VBLAST scheme applied with 16PSK and $N_t = 2$. For the cases of $\alpha = 0.001$ and $\alpha = 0.0001$, though NOMA-VBLAST adopted QPSK and $N_t = 4$ holds a dominance within the moderate SNR regime, NOMA-SM keeps improving its performance with the increase of SNR and outperform the references in terms of higher diversity gain. By jointly considering the above observations, we conclude that NOMA-SM constitutes a potent amalgam.

11.5.2 Capacity Results and Discussions

Below, we evaluate the capacity of the NOMA-SM system associated with different power allocation strategies. All results presented in this subsection are obtained by averaging the instantaneous capacities over multiple channel realizations. In

particular, we fix $K = 0.2$, $\kappa_t = \kappa_r = 0.5$, and $\delta = 1$ unless otherwise stated. For benchmarking, we use an OMA-SM system, where V_1 transmits messages to V_2 using SM in the first slot. Then, V_1 sends messages through the previously activated antenna to U, without activating another antenna. This OMA-SM model constitutes a fair reference for the NOMA-SM system, since the signal intended for V_2 is conveyed by both the APM signal- and Tx-domain, whereas the signal destined for U is only embedded in the classical signal-domain. The distinctive feature of OMA-SM is that data transmissions destined for V_1–V_2 and V_1–U are operated in an orthogonal time division way within the classical APM signal-domain. Accordingly, the capacity upper bound for V_2 and the capacity for U in the OMA-SM system are expressed as

$$\begin{aligned} \mathscr{C}_V^B &= \min\left\{\mathscr{C}_V^{B_1}, \mathscr{C}_V^{B_2}\right\}, \\ \mathscr{C}_U &= \tfrac{1}{2N_t}\sum_{i=1}^{N_t}\log_2\left(1+\tfrac{\alpha E_s}{\sigma_0^2}\|\mathbf{g}_i\|^2\right), \end{aligned} \tag{11.25}$$

respectively, where

$$\begin{aligned} \mathscr{C}_V^{B_1} &= \tfrac{1}{2N_t}\sum_{i=1}^{N_t}\log_2\left(1+\tfrac{(1-\alpha)E_s p_0}{\sigma_0^2}\|\mathbf{h}_i\|^2\right)+\tfrac{1}{2}\log_2(N_t), \\ \mathscr{C}_V^{B_2} &= \tfrac{1}{2}\log_2\det\left[\mathbf{I}+\tfrac{(1-\alpha)E_s p_0}{\sigma_0^2 N_t}\mathbf{H}\mathbf{H}^H\right]. \end{aligned} \tag{11.26}$$

Let us first check the capacity associated with a fixed power allocation, that is $\alpha = 0.01$. Figure 11.9 depicts the capacity of V_2 and U, as well as the sum capacity versus SNR for both NOMA-SM and OMA-SM. Compared to OMA-SM, NOMA-SM provides substantial capacity gains both for the collaboration-aided vehicle V_2 and for the in-car user U and accordingly obtains a significant sum capacity enhancement. Specifically, the capacity C_U has been beneficially boosted by the proposed scheme, about twice as high as that of OMA-SM. Since the APM signal-domain of the proposed scheme is combined with a NOMA strategy, each user accesses the channel resources via power domain multiplexing.

Subsequently, we investigate the efficiency of the proposed power allocation optimization. Specifically, the power allocation optimization denoted by $\mathscr{Q}$ is considered for OMA-SM, which is formulated as

$$\begin{aligned} \mathscr{Q}: \max_{\alpha} \quad & \mathscr{C}_U + \mathscr{C}_V^B \\ s.t. \quad & \begin{cases} \mathscr{C}_U \geq \tilde{\mathscr{C}}_U, \\ \mathscr{C}_V^B \geq \tilde{\mathscr{C}}_V^B, \\ 0 < \alpha < 1. \end{cases} \end{aligned} \tag{11.27}$$

For simplicity, the minimum rate requirements of V_2 and U are set to $\tilde{\mathscr{C}}_U = \frac{\mathscr{C}_U(\alpha=1)}{2}$ and $\tilde{\mathscr{C}}_V^B = \frac{\mathscr{C}_V^B(\alpha=0)}{2}$, which respectively correspond to the lower bound and upper

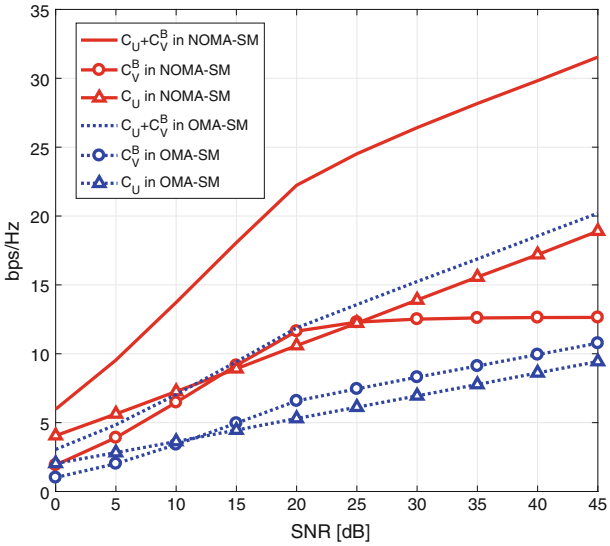

Fig. 11.9 Capacity of V_2 and U, or the sum capacity versus SNR for the NOMA-SM and OMA-SM scheme with a fixed power allocation factor, i.e. $\alpha = 0.01$. Specifically, C_V^B and C_U in NOMA-SM are evaluated from (11.18) and (11.11), while C_V^B and C_U in OMA-SM are obtained from (11.25)

bound of α's feasible set. Then, a full-search algorithm is applied for OMA-SM within the feasible set.

Figure 11.10 illustrates the capacity of V_2 and U for NOMA-SM with optimization $\mathscr{P}$ or $\mathscr{O}$, where the QoS of the collaboration-aided vehicle V_2 and the in-car user U, i.e. $\tilde{C}_V^B$ and $\tilde{C}_U$, are also plotted for reference. It can be observed that C_V^B always meets the requirement of $\tilde{C}_V^B$ with the aid of the optimization $\mathscr{P}$, and C_U associated with the optimization $\mathscr{O}$ exactly meets the QoS $\tilde{C}_U$. This observation is in accordance with the foregoing analysis, which indicates that the optimization $\mathscr{P}$ intends to maximize C_U, while maintaining the QoS $\tilde{C}_V^B$ for V2V transmission, whereas the optimization $\mathscr{O}$ aims for maximizing C_V^B while guaranteeing the minimum rate requirement $\tilde{C}_U$ for the in-car user. Thus, we find that the optimized C_U of $\mathscr{P}$ is higher than that of $\mathscr{O}$, whereas the optimized C_V^B of $\mathscr{O}$ outperforms that of $\mathscr{P}$. Accordingly, the more appropriate optimization scheme can be readily selected based on the data priority of distinct transmission links.

Figure 11.11 compares the results of the optimization $\mathscr{Q}$ to that of $\mathscr{P}$ and $\mathscr{O}$. Let us contrast $\mathscr{P}$ and $\mathscr{Q}$ first. Clearly, both C_V^B and C_U in NOMA-SM with optimization $\mathscr{P}$ have been remarkably improved, demonstrating that the NOMA strategy offers a bandwidth efficiency improvement. By considering the results of $\mathscr{O}$ and $\mathscr{Q}$ in Fig. 11.11, we find that C_U of NOMA-SM associated with optimization $\mathscr{O}$ is tightly lower bounded by that of OMA-SM associated with optimization $\mathscr{Q}$, and C_V^B with $\mathscr{O}$ provides a substantial gain, achieving nearly twice that of $\mathscr{Q}$.

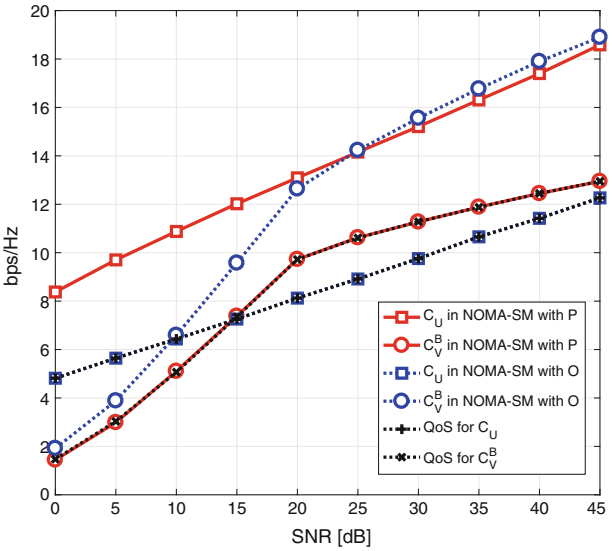

Fig. 11.10 Capacity of V_2 and U, or the respective QoS versus SNR for NOMA-SM with power allocation optimization $\mathscr{P}$ or $\mathscr{O}$. Specifically, C_V^B and C_U in NOMA-SM with $\mathscr{P}$ or $\mathscr{O}$ are evaluated with the aid of the algorithm in Table 11.1. The QoS for C_V^B and C_U, i.e. $\tilde{C}_V$ and $\tilde{C}_U$, are set according to (11.24)

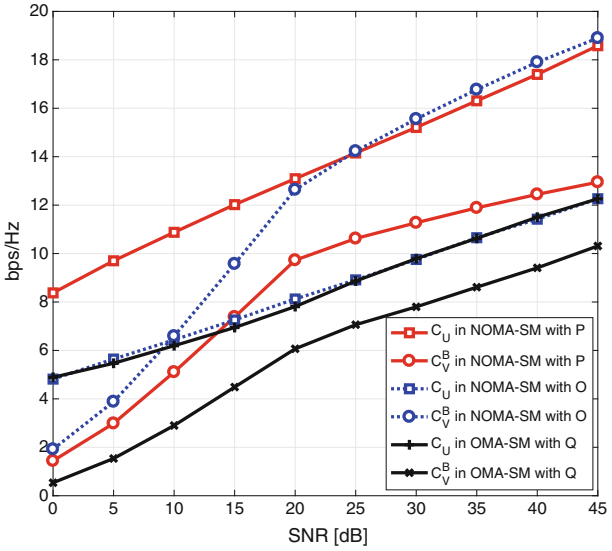

Fig. 11.11 Capacity of V_2 and U versus SNR for NOMA-SM with power allocation optimization $\mathscr{P}$ or $\mathscr{O}$, and OMA-SM with power allocation optimization $\mathscr{Q}$, respectively. Specifically, C_V^B and C_U in NOMA-SM with $\mathscr{P}$ or $\mathscr{O}$ are evaluated with the aid of the algorithm in Table 11.1. While C_V^B and C_U in OMA-SM with $\mathscr{Q}$ are obtained from a full-search algorithm

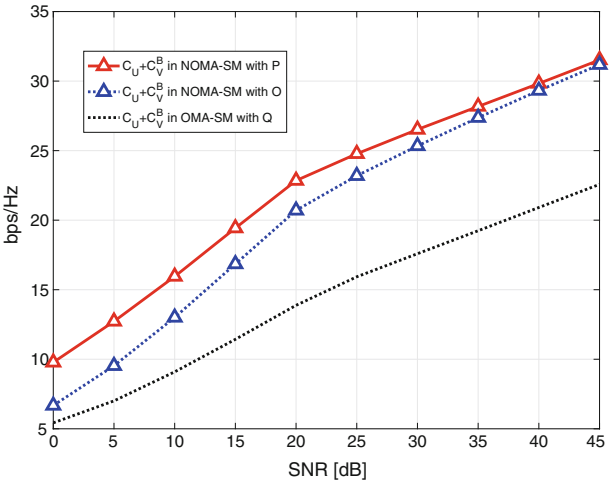

Fig. 11.12 Sum capacity versus SNR for NOMA-SM with power allocation optimization $\mathscr{P}$ or $\mathscr{O}$, and OMA-SM with power allocation optimization $\mathscr{Q}$, respectively. Specifically, C_V^B and C_U in NOMA-SM with $\mathscr{P}$ or $\mathscr{O}$ are evaluated with the aid of the algorithm in Table 11.1. While C_V^B and C_U in OMA-SM with $\mathscr{Q}$ are obtained from a full-search algorithm

Furthermore, it can be observed from Fig. 11.12 that the NOMA-SM systems achieve higher sum capacity than OMA-SM. Specifically, optimization $\mathscr{P}$ provides higher capacity gain than $\mathscr{O}$, since $\mathscr{P}$ aims for maximizing the data rate of the in-car user U, which experiences a much better channel than the collaboration-aided vehicle V_2.

11.6 Chapter Summary and Future Outlook

In this chapter, we introduce NOMA and SM techniques into V2X scenarios in order to support high bandwidth efficiency and enhanced link reliability. The BER performance of the new NOMA-SM transmission strategy has been investigated with the impact of the Rician K-factor, spatial correlation of antenna array, time-varying effect of the V2V channel, and the power allocation factor being discussed. Compared to NOMA relying on VBLAST, NOMA-SM has been demonstrated to exhibit improved robustness against the spatial and temporal effects of the V2V channel. By analysing the capacity and deriving analytical upper bounds in closed form, a pair of power allocation optimization schemes have been formulated for NOMA-SM. The optimal solutions have also been shown to be achievable with the aid of the proposed power allocation algorithm. Our numerical results have verified that with the aid of an appropriate power allocation, NOMA-SM is capable of satisfying the QoS support of a low priority flow, whilst maximizing the throughput of the

high priority flow. In summary, NOMA-SM has been demonstrated to cooperatively improve the link reliability and bandwidth efficiency of V2V transmissions.

Nonetheless, several open issues still need to be carefully addressed before NOMA can be practically exploited in vehicular environments. Here, we discuss two potential research topics in this field as examples.

Parallel Interference Cancellation-Aided NOMA: There is a much broader range of V2X applications to be considered in VANETs, especially within the automated driving field, whose characteristics are more stringent, as captured by the ultra-reliable low-latency constraints. The traditional NOMA schemes use the classic SIC technique, where a high received signal power difference is preferred. However, this condition cannot always be guaranteed, especially in a traffic jam, where all cars tend to have similar channel conditions. Furthermore, SIC receivers were reported to exhibit an error floor in high-order modulation modes due to error propagation across the cancellation stages [60]. By contrast, parallel interference cancellation (PIC) does not require any specific detection order and all users reconstruct the signals of all the other users in parallel. Then, they subtract the reconstructed signals from the composite signal. Hence, PIC outperforms SIC when the received signal powers for all users are similar. With the advent of a PIC receiver, NOMA is expected to possess enhanced transmission reliability as well as better applicability to highly-loaded vehicular scenarios. In a nutshell, the performance analysis of NOMA with PIC should be addressed in our further research.

NOMA for Cognitive V2X: The large amount of data generated by the vehicles might impose excessive traffic demands on traditional cellular traffic. Hence, cognitive NOMA principles can be conceived for delay-tolerant vehicular communications services to opportunistically access the channels originally occupied by the cellular users. Given a dedicated spectral band, cellular users and vehicles can be regarded as primary users and secondary users, respectively. The vehicles would only be permitted to access the channel when the services of cellular users are not affected. In contrast to the traditional cognitive radio scheme, both of the power control and resource allocation need to be designed elaborately, and efficient transmission schemes accommodating both primary and secondary users should be proposed and analysed carefully.

References

1. 3GPP TS 22.185, Service requirements for V2X services, Feb 2016
2. D. Jiang, L. Delgrossi, IEEE 802.11p: towards an international standard for wireless access in vehicular environments, in *Proceedings VTC Spring 2008—IEEE Vehicular Technology Conference* (Singapore, May 2008), pp. 2036–2040
3. S.H. Sun, J.L. Hu, Y. Peng, X.M. Pan, L. Zhao, J.Y. Fang, Support for vehicle-to-everything services based on LTE. IEEE Wirel. Commun. **23**(3), 4–8, June 2016
4. M. Amadeo, C. Campolo, A. Molinaro, Enhancing IEEE 802.11p/WAVE to provide infotainment applications in VANETs. Elsevier Ad Hoc Netw. **10**(2), 253–269 (2012)
5. S. Chen et al., Vehicle-to-everything (v2x) services supported by LTE-based systems and 5G. IEEE Commun. Stand. Mag. **1**(2), 70–76 (2017)

6. S. Chen, J. Hu, Y. Shi, L. Zhao, LTE-V: a TD-LTE-based V2X solution for future vehicular network. IEEE Internet Things J. **3**(6), 997–1005 (2016)
7. 3GPP RP-152293, New WI proposal: support for V2V services based on LTE sidelink, Dec 2015
8. G. Araniti, C. Campolo, M. Condoluci, A. Iera, A. Molinaro, LTE for vehicular networking: a survey. IEEE Commun. Mag. **51**(5), 148–157 (2013)
9. 3GPP TS 23.285, v.14.1.0, Architecture enhancements for V2X services, Dec 2016
10. 3GPP, TS 36.440, General aspects and principles for interfaces supporting multimedia broadcast multicast service (MBMS) within E-UTRAN, Rel. 11, Sept 2012
11. L. Hanzo, O. Alamri, M. El-Hajjar, N. Wu, Near-capacity multi-functional MIMO systems: sphere-packing, iterative detection and cooperation (Wiley, New York, NY, USA, 2009)
12. L. Wang, R. Li, C. Cao, G.L. Stüber, SNR analysis of time reversal signaling on target and unintended receivers in distributed transmission. IEEE Trans. Commun. **64**(5), 2176–2191 (2016)
13. E.G. Larsson, O. Edfors, F. Tufvesson, T.L. Marzetta, Massive MIMO for next generation wireless systems. IEEE Commun. Mag. **52**(2), 186–195 (2014)
14. Y. Wu, R. Schober, D.W.K. Ng, C. Xiao, G. Caire, Secure massive MIMO transmission with an active eavesdropper. IEEE Trans. Inf. Theory **62**(7), 3880–3900 (2016)
15. R. Zhang, Z. Zhong, J. Zhao, B. Li, K. Wang, Channel measurement and packet-level modeling for V2I spatial multiplexing uplinks using massive MIMO. IEEE Trans. Veh. Technol. **65**(10), 7831–7843 (2016)
16. P. Harris et al., Performance characterization of a real-time massive MIMO system with LOS mobile channels. IEEE J. Select. Areas Commun. **35**(6), 1244–1253 (2017)
17. Y. Saito, Y. Kishiyama, A. Benjebbour, T. Nakamura, A. Li, K. Higuchi, Non-orthogonal multiple access (NOMA) for cellular future radio access, in *Proceedings IEEE 77th Vehicular Technology Conference* (Dresden, Germany, June 2013), pp. 1–5
18. Y. Chen, L. Wang, B. Jiao, Cooperative multicast non-orthogonal multiple access in cognitive radio, in *Proceedings 2017 IEEE ICC* (Paris, France, May 2017), pp. 1–6
19. L. Dai, B. Wang, Y. Yuan, S. Han, I. Chih-Lin, Z. Wang, Non-orthogonal multiple access for 5G: solutions, challenges, opportunities, and future research trends. IEEE Commun. Mag. **53**(9), 74–81 (2015)
20. J. Liberti, S. Moshavi, P. Zablocky, Successive interference cancellation. U.S. Patent 8670418 B2, 11 Mar 2014
21. Q. Sun, S. Han, I. Chih-Lin, Z. Pan, On the ergodic capacity of MIMO NOMA systems. IEEE Wirel. Commun. Lett. **4**(4), 405–408, Aug 2015
22. Y. Saito, A. Benjebbour, Y. Kishiyama, T. Nakamura, System-level performance evaluation of downlink non-orthogonal multiple access (NOMA), in *Proceedings IEEE 24th International Symposium Personal Indoor and Mobile Radio Communications (PIMRC)* (London, UK, Sept 2013), pp. 611–615
23. Z. Yang, Z. Ding, P. Fan, N. Al-Dhahir, A general power allocation scheme to guarantee quality of service in downlink and uplink NOMA systems. IEEE Trans. Wirel. Commun. **15**(11), 7244–7257 (2016)
24. L. Lv, J. Chen, Q. Ni, Cooperative non-orthogonal multiple access in cognitive radio. IEEE Commun. Lett. **20**(10), 2059–2062 (2016)
25. K. Au et al., Uplink contention based SCMA for 5G radio access, in *Proceedings IEEE GLOBECOM Workshop* (Austin, TX, Dec, 2014), pp. 900–905
26. B. Di, L. Song, Y. Li, G.Y. Li, Non-orthogonal multiple access for high-reliable and low-latency V2X communications in 5G systems. IEEE J. Select. Areas Commun. **35**(10), 2383–2397 (2017)
27. Y. Chen, L. Wang, Y. Ai, B. Jiao, L. Hanzo, Performance analysis of NOMA-SM in vehicle-to-vehicle massive MIMO. IEEE J. Select. Areas Commun. **35**(12), 2653–2666 (2017)
28. Y. Yang, B. Jiao, Information-guided channel-hopping for high data rate wireless communication. IEEE Commun. Lett. **12**(4), 225–227 (2008)

29. L. He, J. Wang, J. Song, L. Hanzo, On the multi-user, multi-cell massive spatial modulation uplink: how many antennas for each user? IEEE Trans. Wirel. Commun. **16**(3), 1437–1451 (2017)
30. D.A. Basnayaka, M. Di Renzo, H. Haas, Massive but few active MIMO. IEEE Trans. Veh. Technol. **65**(9), 6861–6877 (2016)
31. Y. Chau, S.-H. Yu, Space modulation on wireless fading channels, in *Proceedings IEEE Vehicular Technology Conference—Fall*, vol. 3 (Atlantic City, NJ, Oct 2001), pp. 1668–11671
32. R. Mesleh, H. Haas, C. W. Ahn, S. Yun, Spatial modulation—a new low complexity spectral efficiency enhancing technique, in *Proceedings 2006 First International Conference on Communications and Networking in China* (Beijing, 2006), pp. 1–5
33. R.Y. Mesleh, H. Haas, S. Sinanovic, C.W. Ahn, S. Yun, Spatial modulation. IEEE Trans. Veh. Technol. **57**(4), 2228–2241 (2008)
34. J. Jeganathan, A. Ghrayeb, L. Szczecinski, Spatial modulation: optimal detection and performance analysis. IEEE Commun. Lett. **12**(8), 545–547 (2008)
35. T.L. Narasimhan, P. Raviteja, A. Chockalingam, Large-scale multiuser SM-MIMO versus massive MIMO, in *Proceedings, Information Theory and Applications Workshop (ITA)* (San Diego, CA, 2014), pp. 1–9
36. S. Wang, Y. Li, M. Zhao, J. Wang, Energy-efficient and low-complexity uplink transceiver for massive spatial modulation MIMO. IEEE Trans. Veh. Technol. **64**(10), 4617–4632 (2015)
37. P. Patcharamaneepakorn et al., Spectral, energy, and economic efficiency of 5G multicell massive MIMO systems with generalized spatial modulation. IEEE Trans. Veh. Technol. **65**(12), 9715–9731 (2016)
38. L. He, J. Wang, J. Song, On massive spatial modulation MIMO: spectral efficiency analysis and optimal system design, in *Proceedings IEEE GLOBECOM* (2016), pp. 1–6
39. M. Di Renzo, H. Haas, A. Ghrayeb, S. Sugiura, L. Hanzo, Spatial modulation for generalized MIMO: challenges, opportunities, and implementation. Proc. IEEE **102**(1), 56–103 (2014)
40. M. Zhang, X. Cheng, L.Q. Yang, Differential spatial modulation in V2X, in *Proceedings 2015 9th European Conference on Antennas and Propagation (EuCAP)* (Lisbon, Apr 2015), pp. 1–5
41. Y. Fu et al., BER performance of spatial modulation systems under 3-D V2V MIMO channel models. IEEE Trans. Veh. Technol. **65**(7), 5725–5730 (2016)
42. K.P. Peppas, P.S. Bithas, G.P. Efthymoglou, A.G. Kanatas, Space shift keying transmission for intervehicular communications. IEEE Trans. Intell. Transp. Syst. **17**(12), 3635–3640 (2016)
43. Y. Cui, X. Fang, Performance analysis of massive spatial modulation MIMO in high-speed railway. IEEE Trans. Veh. Technol. **65**(11), 8925–8932 (2016)
44. T. Wang, L. Song, Z. Han, Coalitional graph games for popular content distribution in cognitive radio VANETs. IEEE Trans. Veh. Technol. **62**(8), 4010–4019 (2013)
45. H. Ilhan, I. Altunbas, M. Uysal, Optimized amplify-and-forward relaying for vehicular ad-hoc networks, in *Proceedings IEEE Vehicular Technology Conference* (Calgary, BC, Sept 2008), pp. 1–5
46. K. Huang, V.K.N. Lau, Y. Chen, Spectrum sharing between cellular and mobile ad hoc networks: transmission-capacity trade-off. IEEE J. Select. Areas Commun. **27**(7), 1256–1267 (2009)
47. T. Lakshmi Narasimhan, P. Raviteja, A. Chockalingam, Generalized spatial modulation in large-scale multiuser MIMO systems. IEEE Trans. Wirel. Commun. **14**(7), 3764–3779 (2015)
48. Y. Chen, L. Wang, Z. Zhao, M. Ma, B. Jiao, Secure multiuser MIMO downlink transmission via precoding-aided spatial modulation. IEEE Commun. Lett. **20**(6), 1116–1119 (2016)
49. L. Wang, S. Bashar, Y. Wei, R. Li, Secrecy enhancement analysis against unknown eavesdropping in spatial modulation. IEEE Commun. Lett. **19**(8), 1351–1354 (2015)
50. O. Delangre, S. Van Roy, P. De Doncker, M. Lienard, P. Degauque, Modeling in-vehicle wideband wireless channels using reverberation chamber theory, in *Proceedings 2007 IEEE 66th Vehicular Technology Conference* (Baltimore, MD, Oct 2007), pp. 2149–2153
51. X. Cheng, C.X. Wang, D.I. Laurenson, S. Salous, A.V. Vasilakos, An adaptive geometry-based stochastic model for non-isotropic MIMO mobile-to-mobile channels. IEEE Trans. Wirel. Commun. **8**(9), 4824–4835 (2009)

52. M. Koca, H. Sari, Performance analysis of spatial modulation over correlated fading channels, in *Proceedings, IEEE Vehicular Technology Conference (VTC Fall)* (Quebec City, QC, Sept 2012), pp. 1–5
53. J.P. Kermoal, L. Schumacher, K.I. Pedersen, P.E. Mogensen, F. Frederiksen, A stochastic MIMO radio channel model with experimental validation. IEEE J. Select. Areas Commun. **20**(6), 1211–1226 (2002)
54. S.L. Loyka, Channel capacity of MIMO architecture using the exponential correlation matrix. IEEE Commun. Lett. **5**(9), 369–371 (2001)
55. C. Liu, M. Ma, Y. Yang, B. Jiao, Optimal spatial-domain design for spatial modulation capacity maximization. IEEE Commun. Lett. **20**(6), 1092–1095 (2016)
56. X. Guan, Y. Cai, W. Yang, On the mutual information and precoding for spatial modulation with finite alphabet. IEEE Wirel. Commun. Lett. **2**(4), 383–386 (2013)
57. Z. An, J. Wang, J. Wang, S. Huang, J. Song, Mutual information analysis on spatial modulation multiple antenna system. IEEE Trans. Commun. **63**(3), 826–843 (2015)
58. Y. Toor, P. Muhlethaler, A. Laouiti, A.D. La Fortelle, Vehicle Ad Hoc networks: applications and related technical issues, IEEE Commun. Surv. Tutor. **10**(3), 74–88, Third Quarter (2008)
59. S. Boyd, L. Vandenberghe, *Convex Optimization* (Cambridge Univ. Press, Cambridge, U.K., 2004)
60. L. Hanzo, L.-L. Yang, E.-L. Kuan, K. Yen. Single-and multi-carrier DS-CDMA: multi-user detection, space-time spreading, synchronisation, standards and networking (Wiley, 2003)